# Enantiopure Cryptophane Derivatives: Synthesis and Chiroptical Properties

Orsola Baydoun, Thierry Buffeteau, T. Brotin

# Enantiopure Cryptophane Derivatives: Synthesis and Chiroptical Properties

Orsola Baydoun, Thierry Buffeteau, Thierry Brotin*

**Abstract:** This review addresses the synthesis of enantiopure cryptophane and the study of their chiroptical properties. Cryptophane derivatives represent an important class of macrocyclic compounds that can bind a large range of species in solution under different conditions. The overwhelming majority of these host molecules is chiral and their chiroptical properties have been thoroughly investigated. The first part of this review is dedicated to the optical resolution and the synthesis of enantiopure cryptophane derivatives. In a second part, the study of the chiroptical properties of these molecular hosts by different techniques such as electronic and vibrational circular dichroism and Raman optical activity is detailed. These techniques allow the determination of the absolute configuration of cryptophane derivatives and provide useful information about their conformation in different conditions.

**Keywords:** macrocyclic compounds, absolute configuration, ECD, VCD, ROA.

## *1.* Introduction

Cryptophane is the common name, coined by A. Collet in 1985,[1] to describe a class of hollow organic compounds that can reversibly trap and isolate a molecule or an atom from the bulk.[2,3]. Cryptophane derivatives have a characteristic globular shape, which is obtained by joining two cyclotribenzylene (CTB) skeletons by at least three linkers whose nature and length can be varied. This simple structure permits to use a large number of combinations to prepare cryptophane derivatives with specific molecular recognition properties. For instance, cryptophane derivatives bearing organic or inorganic bridges have been reported in literature and their binding properties have been thoroughly studied.[4,6] Besides their interesting binding properties, the overwhelming majority of these host molecules is chiral. The chirality of these molecules is a resultant of their structure, and not due to a stereocenter. The term inherent chirality has been used to characterize the structure of these optically active derivatives by analogy with the study of Böhmer and co-workers to characterize calix-[4]-arene derivatives, which are compounds characterized by a curvature in space. [7] The inherent chirality of cryptophane derivatives is known for a long time since the structure of cryptophane-A (**1**), the first cryptophane ever synthesized, has been identified.[2] However, their chiroptical properties haven't been investigated in details. A. Collet and co-workers pioneered this work in the 80's, in which they reported few articles describing enantiopure cryptophanes and their chiroptical properties using Electronic Circular Dichroism (ECD) spectroscopy. The large majority of articles dealing with the thorough study of the chiroptical properties of cryptophane derivatives appeared after 2000. Both the difficulties to separate the two enantiomers of chiral cryptophanes and to obtain them in fair quantities explain the reasons why the study of their chiroptical properties has been delayed.

In this review, after defining the relative and absolute configuration of cryptophanes (section 2), we will focus on the synthesis (section 3) and the chiroptical properties (section 4) of enantiopure cryptophanes. Different approaches have been used to obtain these molecules in their enantiopure form. For instance, optically active cryptophane derivatives have been first obtained from enantiopure CTB following a multi-step procedure. Thus, section 3.1 will be dedicated to describe the optical resolution of CTB used to prepare optically active cryptophane derivatives. Among the different enantiopure CTB derivatives reported in literature, we will exclusively discuss the synthesis of tris-functionalized CTB derivatives ($C_3$-symmetry), which are prone to prepare cryptophane or hemi-cryptophane derivatives. In this section, we also report the synthesis of enantiopure tribenzotriquinacenes (TBTQ) derivatives (section 3.1; Fig 12) with $C_3$-symmetry, which are potential building blocks for new cryptophane structures with interesting properties. These molecules have a very similar skeleton to CTB derivatives. Then, section 3.2 reports the synthesis of various enantiopure cryptophanes from enantiopure CTB derivatives. Separation of cryptophane diastereomers is another approach to prepare enantiopure cryptophanes and it will be detailed in section 3.3. This approach was successfully applied to prepare a series of cryptophane derivatives with high enantiomeric excess (ee). Finally, when the previous approaches are ineffective, the separation of enantiomers of cryptophane derivatives can be achieved by HPLC using chiral stationary phase, as shown in section 3.4. This analytical tool allowed the separation of numerous cryptophane derivatives, with different shapes and symmetries, using commercially available chiral stationary phases. The two last sections of this review detail the chiroptical properties of enantiopure cryptophanes (section 4) and their complexes (section 5). Chemists now possess a large panel of chiroptical techniques to determine the absolute configuration (AC) of cryptophane derivatives or to gain information about their molecular conformation in solution. For instance, Vibrational Circular Dichroism (VCD) and Raman Optical Activity (ROA) are powerful chiroptical tools to characterize chiral organic compounds in solution. Combined with quantum calculations at the density functional theory (DFT) level, these spectroscopic techniques have been used to determine the AC of cryptophane derivatives with confidence. These techniques also provide valuable information about the conformation adopted by the three

linkers in solution. Additional chiroptical tools such as Electronic Circular Dichroism (ECD), Specific Optical Rotation (SOR) or Optical Rotatory Dispersion (ORD) and X-ray crystallography have been widely used to characterize enantiopure cryptophanes under various experimental conditions.

### *2.* Relative and absolute configuration of cryptophanes

The determination of the relative and absolute configuration is a prerequisite condition before studying the physical properties of these molecules and their complexes. The relative configuration refers to the assignment of the *syn* or *anti* configuration of the cryptophane, and it is directly related to the way the three linkers connect the two CTB scaffolds. Thus, the *anti*-configuration refers to the helicoidal arrangement of the three linkers. Consequently, in all cases, *anti*-cryptophanes are chiral compounds. *Anti*-cryptophane-A, *anti*-**1**, which has a $D_3$-symmetry, (Figure 1, top left) belongs to this class of compound. The *anti*-cryptophane-**2** decorated with twelve methoxy groups represents another example of cryptophane derivative with $D_3$-symmetry (Figure 1, top right). In contrast, the non-helicoidal arrangement of the linkers gives rise to a plane of symmetry ($C_{3h}$-symmetry) in the molecule, and the compound becomes achiral (Figure 1, bottom). The compound presented in Figure 1 (bottom left), which is the diastereomer of *anti*-**1**, has been named as *syn*-cryptophane-B, *syn*-**3**, and its synthesis has been reported only recently.[8] A similar conclusion can be drawn for the *syn*-cryptophane-**4**, bearing twelve methoxy groups (Figure 1, bottom right).[9] This compound is the diastereomer of compound *anti*-**2**.

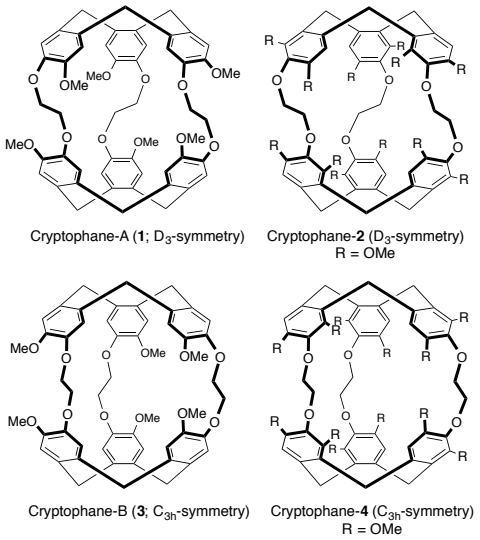


FIGURE 1: Structure of *anti*-cryptophane-A (**1**; chiral), *anti*-cryptophane-**2** (chiral), *syn*-cryptophane-B (**3**; achiral) and *syn*-cryptophane-**4** (achiral). A single enantiomer (*PP*) is given for compounds **1** and **2**. A single enantiomer (*MP*) is given for compounds **3** and **4**. In both cases the first letter *M* or *P* refers to the CTB on top.

It is noteworthy, that compounds **1**, **3** and **2**, **4** possess the same substituents on the two CTB caps. However, the molecule loses its symmetry when the two CTB mioieties are decorated with different substituents. Thus, cryptophane derivatives bearing different CTB are chiral regardless their configuration (*anti* or *syn*). As examples, we can mention *anti*-cryptophane C, *anti*-**5**, and syn-cryptophane D, *syn*-**6**, that both possess $C_3$-symmetry (Figure 2, top),[1] or the *anti*-cryptophane-**7** and *syn*-cryptophane-**8** bearing nine methoxy substituents (Figure 2, middle).[9] Other systems with two different CTB scaffolds have been reported in literature in their racemic form.[10,11,12,13,14] Decreasing the molecular symmetry from $D_3$ to $C_1$ leads, in all cases, to *anti* or *syn* cryptophane derivatives that possess an inherent chiral structure. The monofunctionalized cryptophane bearing a single phenol function is probably the best example since this derivative has been widely used both in its racemic or enantiopure forms to build up more complicated scaffolds for biosensing applications.[15,16,17] Finally, *anti*-cryptophane derivatives with $C_2$-symmetry also have an inherent chiral structure. Such compounds can be obtained by introducing two linkers of different nature into the cryptophane skeleton. The so-called *anti*-cryptophane-223, *anti*-**9**, and *anti*-cryptophane-233, *anti*-**10**, belong to this class of compounds (Figure 2, bottom).[18]

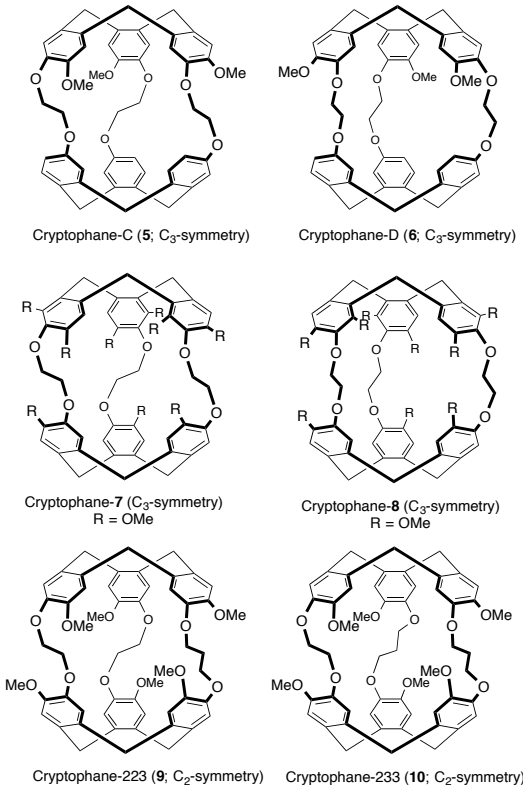


FIGURE 2: Structure of anti-cryptophane-C (**5**; chiral), *syn*-cryptophane-D (**6**; chiral), *anti*-cryptophane-**7** (chiral), *syn*-cryptophane-**8** (chiral), *anti*-cryptophane-223 (**9**; chiral) and *anti*-cryptophane-233 (**10**; chiral).

It should be noted that the *anti* and *syn* compounds, with a few exceptions, are usually obtained, in different amounts, during the same synthetic step. Thus, the rapid identification of the *syn*- and *anti*-derivatives can be difficult because the two diastereomeric compounds usually present large similarities in their $^{1}H$ and $^{13}C$ NMR spectra. In the past, different techniques have been used to identify the *syn*- and *anti*-cryptophanes. For instance, HPLC on chiral stationary phase is widely used to distinguish between achiral *syn*- (one single peak) and chiral *anti*-cryptophanes (two distinct peaks).[19] When X-ray crystals are rapidly available, X-ray crystallography is the definitive tool to attribute the *syn* or *anti* configuration of cryptophane derivatives. For instance, single crystals of cryptophane-D, **6**, have been obtained from a mixture of $CH_2Cl_2$ and acetone. Interestingly, in this example, the X-ray structure revealed that the lattice contained a single enantiomer (spontaneous resolution).[20] If X-ray crystals cannot be obtained, optical resolution of the stereoisomers is done, followed by the study of their chiroptical properties, specifically by VCD spectroscopy combined with quantum calculations at the DFT level. The latter techniques have been used to assign the relative configuration of compounds **7** and **8** (both chiral compounds) bearing 9 methoxy substituents.[21]

The stereochemistry of enantiopure cryptophanes can be assigned using the nomenclature suggested by V. Prelog for the specification of the absolute configuration (AC) of $C_3$-CTB derivatives, in accordance with IUPAC rules (i.e. using the stereo-descriptors *M* or *P*).[22,23] Thus, to determine the AC of a $C_3$-symmetric CTB bearing two different chemical groups X and Y, it is sufficient to choose one of the three equivalent pairs of two aromatic rings and their corresponding methylene bridge, [(C(5), C(10) or C(15)], as shown in Figure 3. For instance, let's consider, the pair h-C(15) and a-C(15), and draw its Newman projection. This representation allows to define two resultant torsion angles, τ (g-h-C(15)-a) and τ' (b-a-C(15)-h). The choice between the two torsion angles depends on the priority of the X and Y substituents and will subsequently determines the absolute configuration. So, if group Y has higher priority over X, then Newman scheme A has to be selected (Y is closer to h than to a), and consequently the CTB will have the M conformation. The opposite situation (X>Y) will give rise to the P conformer. It's worth mentioning that the current example is the simplest to be considered, and more complicated attribution is expected in case of $C_1$-CTB bearing different substituents.

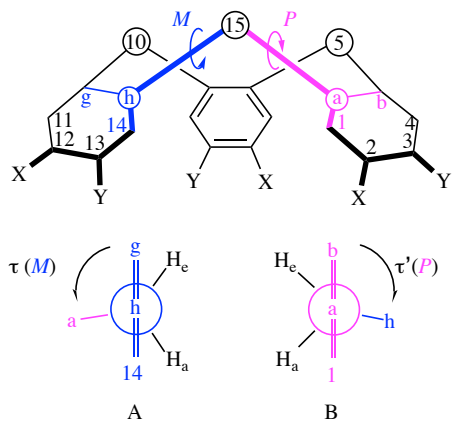


FIGURE 3: Prelog's representation for the assignment of the *M* or *P* absolute configuration of $C_3$-CTB derivatives bearing two substituents (X and Y). $H_a$ and $H_e$ refer to the axial and equatorial protons attached to C(15). Reproduced from Ref. 22 with permission from The Royal Society of Chemistry.

Using this nomenclature, we can easily assign the stereo-descriptor of the enantiomer of cryptophane-**1** shown in Figure 1 (top, left). This cryptophane is made of two CTB moieties that possess the same absolute configuration *P*, and consequently its stereo-descriptor will be *PP*. In contrast, the enantiomer of *syn*-cryptophane-B, *syn*-**3**, shown in Figure 1 (bottom, left) possesses two caps of opposite absolute configuration *M* and *P*, and the stereo-descriptor of this compound will be *PM* or *MP* due to its *meso* form.

## *3.* Synthesis of chiral cryptophanes

### 3.1. Synthesis of optically active cyclotribenzylene (CTB)

Enantiopure cyclotribenzylenes of $C_3$-symmetry bearing three reactive functions appear as the simplest building blocks to prepare optically active cryptophane derivatives. Thus, in this section, we will describe the different approaches to obtain these derivatives in their enantiopure form. Two main methods have been developed to resolve these compounds: the synthesis of CTB diastereomers followed by their separation and hydrolysis to get the enantiomers, and the separation of racemic CTB mixture by HPLC using chiral stationary phases.

CTB derivatives are synthesized from three consecutive Friedel-Crafts alkylations of electron rich 3-4-disubstituted benzyl alcohols derivatives (usually vanillic alcohols), which adopt preferentially a crown-shaped conformation (Figure 4). Depending on its substituents, CTB derivatives can have an achiral $C_{3v}$-symmetry if all the substituents on the CTB rims are identical or a chiral $C_3$- or $C_1$-symmetry if they are different in nature. The two enantiomers of the chiral CTB derivatives possess helical chirality; hence, they can adopt an *M* or a *P* helicity.[3,24] It has been shown, that the interconversion between the two enantiomers (*M* and *P*) easily takes place above room temperature due to the low inversion barrier ($\Delta G^* \approx 110$-$115$ kJ/mol).[25] Other CTB-derived structures show the same inversion barrier.[3,26] The calculated lifetimes ($t_{1/2}$) for racemization are in the order of 960 days, 36 days, and 3 min at 0, 20 and 100°C, respectively. High temperature presents the main drawback to produce enantiopure CTB derivatives. Nevertheless, enantioenriched CTB derivatives with high ee can be obtained at room temperature, allowing further characterizations.

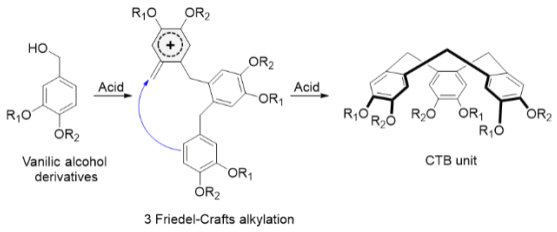


FIGURE 4: Synthesis of CTB derivatives (crown-shape conformation) from the corresponding vanilic alcohol derivative under acidic conditions by three consecutive Friedel-Crafts alkylation.

The first method to obtain optically active CTB involves the trimerization of a properly functionalized enantiopure starting materials bearing a chiral auxiliary. This trimerization step results in the formation of two diastereomeric species, which can be readily separated at room temperature by chromatography on silica gel. Recovery of the desired enantiopure CTB is then achieved by applying mild multi-step reactions. For example, Collet and co-workers reported the synthesis of the two enantiopure cyclotriguaicylene (CTG) *M*-**11** and *P*-**11** derivatives

using α-bromo-propanoic acid as the chiral auxiliary.[27] The first step involved the cyclisation of the enantiopure vanillic alcohol derivative **12**, in $HClO_4$ (65%). This step afforded a diastereomeric mixture of the two CTB-**13** compounds. An additional esterification step using diazomethane allowed the access of the two separated CTB-**14** diastereomers. These two diastereomers were subjected to subsequent reactions to give the desired enantiopure cyclotriguaicylene **11** (Figure 5).

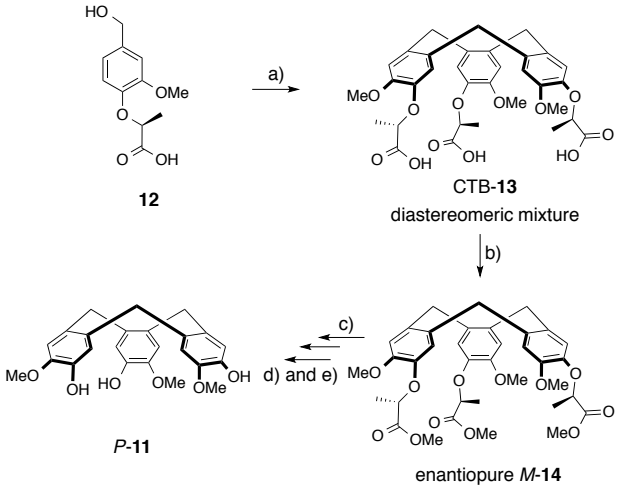


FIGURE 5: Synthesis of enantiopure CTG **11** derivative from enantiopure vanillic alcohol derivative **12**. a) $HClO_4$, 65%, b) $CH_2N_2$, 32% c) $LiAlH_4$, THF, 99% d) MsCl, pyridine, 87% then $MgI_2$, ether/ $CH_2Cl_2$ 69% e) Zn, $CH_3CO_2H$, 91%.

Following the same approach, the two enantiomers of $C_3$-cyclotriphenolene **16**,[28] bearing three phenol functions have been synthesized and separated starting from a sulfur-substituted CTB derivative, **15**.[29] After applying several chemical transformations, mainly desulfurization and demethylation steps, the enantioenriched CTB-**16** was obtained in a quantitative yield, (Figure 6). It is worth mentioning that this derivative is the main building block for the synthesis of the enantioenriched *anti*-**5**. This approach revealed the usefulness of enantiopure sulfur-substituted CTB in the elaboration of other CTB derivatives.

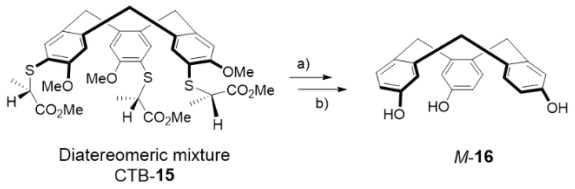


FIGURE 6: Synthesis of cyclotriphenolene **16** from CTB **15**. a) Raney Nick, EtOH/THF, 94%, b) $BBr_3$, $CH_2Cl_2$, 100%.

Other enantiopure CTB derivatives have been obtained from a slightly modified procedure. Indeed, their synthesis relies on the reaction of a readily trimerized CTB with a chiral auxiliary to form two diastereomers, which can be separated by chromatography on silica gel. This method is considered as a straightforward approach to get enantioenriched CTB derivatives in gram-scale. Various chiral auxiliaries were used for this purpose, including ω-camphanic acid, (*R*)-(+)-2-phenoxypropanoic acid or (*R*)-(+)-2-(4-chlorophenoxy)-propionic acid, which are mildly removed after the separation.[3,25,30,31,32,33]For example, the coupling of a racemic sulfur-substituted CTB, *rac*-**17**, with (*R*)-(+)-2-(4-chlorophenoxy) propionic acid **18**, using DCC and dimethyl-amino-pyridine (DMAP) at room temperature afforded a mixture of two diastereomers **19** (Figure 7). This mixture was easily separated by chromatography on silica gel offering the two isomers with high diastereomeric excess de > 95%. The chiral auxiliary was successfully removed by a mild reductive elimination using $LiAlH_4$ at 0 to 20 °C. This reaction was selected instead of the usual saponification to prevent the racemization at higher temperature. The two enantiomers *M*-**17** and *P*-**17** were obtained in high ee > 95%.

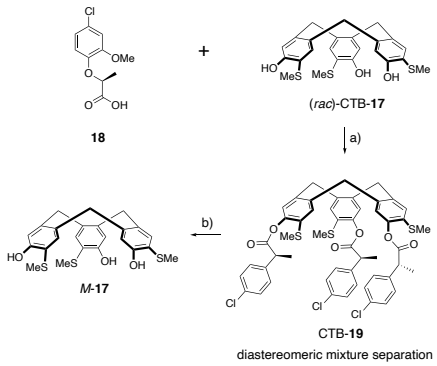

FIGURE 7: Synthesis of enantiopure sulfur-containing CTB *M*-**17** and *P*-**17** using (*R*)-(+)-2-(4-chlorophenoxy) propionic acid **18** as a chiral auxiliary. a) DCC, DMAP, $CH_2Cl_2$ 38% b) $LiAlH_4$, THF, 91%. Only the enantiomer M-**17** is shown.

Using a similar strategy, Zheng and co-workers reported the synthesis of enantiopure $C_3$-symmetric CTB derivative with three phenol and three aryl functions, **20** using (-)-ω-camphanic acid chloride as a chiral auxiliary (Figure 8).[34] It is important to highlight that a family of this CTB derivatives have been obtained from a convenient palladium-catalyzed Suzuki–Miyaura coupling reaction between a tris-brominated CTB **21** and aryl or heteroaryl boronic acids. These molecules are fluorescent and their optical properties vary upon fullerene-60 complexation.

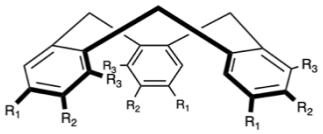

| CTB | $R_1$ | $R_2$ | $R_3$ |
|---|---|---|---|
| **20** | Ph | OH | H |
| **21** | Br | OMe | H |
| **22** | OMe | OMe | OMe |
| **23** | OMe | $C_2H_4Br$ | H |
| **24** | OMe | $C_2H_4OH$ | H |

FIGURE 8: Structure of CTB derivatives and their substituents.

Chiral HPLC has also been used to obtain enantiopure CTB derivatives. This method gained a great attention since it does not necessarily require chemical transformations. The main disadvantages of this technique are its limitation to small-scale separation, the high cost of semi-preparative columns and large volumes of mobile phase. This method also requires optimization of the separation conditions that can be difficult and time consuming in some cases. Solubility issues of the racemic material have also to be taken into consideration. In Collet's first example, racemic mixtures of various CTB derivatives were successfully separated on Chiralpak OT-(+) as a stationary phase with ee ≥ 90%.[19] Although efficient, Chiralpak OT-(+) suffers from low stability over time that leads to a degradation of its performance. Since then, this stationary phase was replaced by more stable chiral stationary phases such as Welk-O1 and Chiralpak IA-IE columns.

The two enantiomers of a $C_3$-symmetrical CTB derivative decorated with nine methoxy groups, CTB **22** were separated by chiral HPLC using a Chiralcelod-H column.[35] In this separation, and upon heating the mixture, it was also possible to detect 25% of a second $C_1$-symmetric isomer known as the saddle-conformer. The two enantiomers of the saddle conformer were not separated because of the fast pseudo-rotation. The physical properties of the two conformational isomers, i.e. the crown and saddle were studied in their racemic forms. In addition, the chiroptical properties of the crown CTB compound were thoroughly investigated in the same study using ECD and VCD spectroscopy.[35] Recently, a similar study was conducted on CTB-**16** (shown in Figure 6), for which its enantiomers were separated by chiral HPLC using Chiralpak IB column.[36] Interestingly, successful separation of the saddle conformer was made possible using a (*S*,*S*)-Whelk-O1 column as the stationary phase. This separation enabled the authors to determine the relative ratios of these species directly and hence follow the racemization process. The isolated saddle conformer was fully characterized by $^1H$ and $^{13}C$ NMR spectroscopy.

It is noteworthy that Martinez and co-workers recently reported a successful gram-scale preparation of the two enantiomers of a CTB **23** derivative bearing pendant bromo ethyl chains by using semi-preparative chiral HPLC (Figure 9).[37] This was realized using chiral HPLC specifically on a Chiralpak ID column with ee > 99.5%. The enantiopure CTB units were obtained only in four steps and in a few days, reflecting the utility of such a method. Then, different aromatic linkers have been grafted to this CTB to design various enantiopure hemicryptophane derivatives without loss of ee. Hemicryptophane is a chiral ditopic molecular cage used extensively in catalysis, receptors and molecular machines, whose properties have been recently reviewed.[38,39]

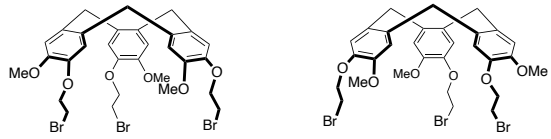

*M*-**23** *P*-**23**

FIGURE 9: CTB *M*-**23** and *P*-**23** separated on Chiralpak IB (Heptane/EtOH/$CHCl_3$: 70/10/20) at 298 K. $t_1$ = 9.01 min for *P*-**23**, $t_2$ = 10.97 min for M-**23** (α = 1.33; Rs = 3.22).

Similarly, Diederich and co-workers reported the synthesis of CTB **24** derivative functionalized by three ethyl alcohol groups (Figure 8).[40] This compound have been effectively resolved by HPLC on (*S*,*S*)-Whelk-O1 chiral stationary phase. Further chemical transformation led to a derivative that was then grafted to fullerene-60 by a triple Bingel addition reaction, giving four enantiopure isomers, whose structures and absolute configurations were assigned by NMR, ECD and VCD spectroscopy, associated with DFT and TD-DFT calculations.

While most of the described CTB derivatives possess $C_3$- or $C_{3v}$-symmetry, $C_1$-symmetric trimers are more challenging to obtain and little contribution has been reported in this field. In a recent study, Martinez and co-workers reported an original approach to synthesize $C_1$-symmetric CTB derivativess.[41] The initial $C_3$-symmetry was broken by inverting the positions of two alkoxy groups on one of the aromatic rings (Figure 10). A mixture of $C_1$-

(**25**) and $C_3$-symmetric (**26**) CTB compounds were obtained by the cyclisation of the two appropriate regio-isomers using scandium triflate, in a total yield of 51%. The enantiomers of these CTB derivatives were separated on Chiralpak IB column HPLC (Heptane/EtOH/$CH_2Cl_2$: 75/5/20) with high ee (> 98.5 %), and their chiroptical properties were studied by ECD spectroscopy. The removal of the three allyl moieties under smooth condition give rise to the two enantiomers *M*-**11** and *P*-**11** in good yields.

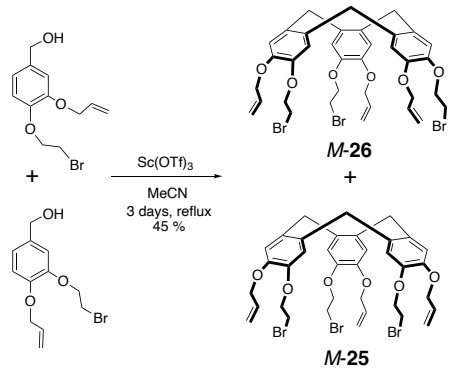


FIGURE 10: Synthesis of $C_1$-symmetric CTB-**25** and $C_3$-symmetric CTB-**26**. Optical resolution was achieved by Chiral HPLC. Only a single enantiomer is shown for each compound **25** and **26**.

An alternative approach to obtain CTB with high ee was developed by Warmuth and co-workers, using a thermodynamic dynamic resolution.[42] The imination of a racemic mixture of CTB **27** derivative functionalized by three aldehydes with two equivalents of (*R*,*R*)-diaminocyclohexane, **28** offered a unique (*P*,*P*,*R*,*R*,*R*)-cryptophane enantiomer **29** in an excellent 92% yield (Figure 11). In fact, the high reaction temperature and thermodynamic sink of the obtained cryptophane enantiomer were the main reasons of this complete inversion. Hydrolysis of compound **29** in a mixture of trifluoroacetic acid and water gave the enantiopure *P*-**27** in 92% yield with ee > 99%.

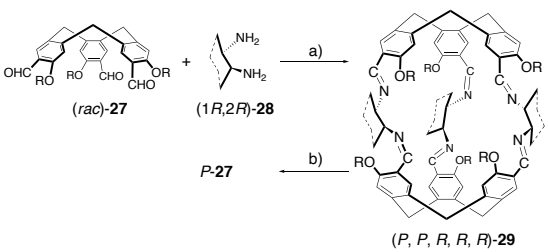


FIGURE 11: Optical resolution of CTB **27** by the synthesis of (*P*,*P*,*R*,*R*,*R*)-cryptophane-**29**, followed by a hydrolysis under acidic conditions. a) cat. TFA in $CHCl_3$, 92% b) TFA, $H_2O$, 92%.

Enantiopure tribenzotriquinacenes (TBTQ) represent another class of interesting compounds whose structure is close to that of CTB derivatives. These compounds can be considered as CTB congeners in which an alkane bridge fuses the three methylene moieties. The synthesis of enantiopure TBTQ derivatives with only $C_3$-symmetry will be reported in the next paragraphs, since these compounds can be used to prepare enantiopure capsules-type cryptophanes.

Kuck and co-workers pioneered the synthesis of these original structures since 2006.[43,44] Compared to CTB derivatives, TBTQ feature similar symmetry and shape but they exhibit greater rigidity thanks to the bridge fusing the three methylene groups. Interestingly, this enhanced rigidity makes them resistant to temperature-induced racemization. However, these molecules are usually harder to obtain in their $C_3$-symmetry and this may explain why they have not been yet largely employed to build-up molecular capsule. Nevertheless, some examples have been recently reported to build-up covalently bound container molecules like cryptophanes or self-organized supramolecular structures.[45] For instance, Kuck and co-workers reported a novel synthetic approach to get tri-ortho-substituted TBTQ. Starting with properly functionalized Knoevenagel adducts like trifunctionalized ortho-substituted-phenyl diols, the reaction allowed the regiospecific synthesis of various ortho-functionalized tribenzotriquinacenes possessing $C_3$-symmetry. These TBTQ derivatives were successfully separated by chiral HPLC.[46] Other $C_3$-symmetric 2,6,10-trisubstituted units have been also reported by employing two regioselective synthetic pathways, namely the Kuck's procedure or the double cyclisation and the Hopf's procedure. Using these procedures, different variants of TBTQ were synthesized. The enantiomers of these units were optically resolved on Chiralpak IB HPLC column (Hexane/isopropanol) with high ee.[47,48] Some of these TBTQ were recently used to construct enantiomerically pure TBTQ dimers bearing platinum diacetelyne units. The absolute configurations of the dimers were determined by ECD spectroscopy and X-ray crystallographic analysis of their crystals.[49]

Mastalerz and co-workers reported a $C_3$-symmetric TBTQ **30** derivative bearing three amino groups (Figure 12).[50] This compound was obtained in its enantiopure form by an efficient formation of diastereomeric salts with tartaric acid. For example, *P*-TBTQ **30** precipitates in the presence of dibenzoyl-D-tartaric acid in ethyl acetate. Similarly, *M*-enantiomer precipitates with dibenzoyl-L-tartaric acid. A neutralization step affords the two enantiomers in high ee > 99%. TBTQ *P*-**30** was then transformed to TBTQ *P*-**31** triodide derivative over two steps in 71% yield. This step highlights the usefulness of the TBTQ **30** as an intermediate to build new enantiopure TBTQ derivatives.

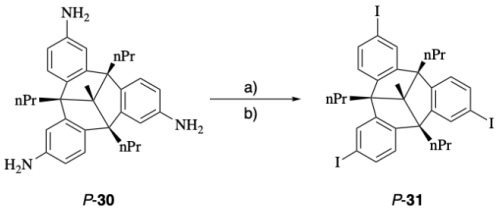


*P*-**30** *P*-**31**

FIGURE 12: Synthesis of TBTQ P-**31** starting from TBTQ *P*-**30**. a) $NaNO_2$, HCl, $H_2O$, b) KI, $H_2O$, (overall yield: 71%).

The same group reported a scalable optical resolution of a $C_3$-symmetric TBTQ derivative by solvent-controlled fractional crystallization of diastereomeric mixtures.[51] The first step involved an esterification of TBTQ triol **32** with (1*S*)-(-)-camphanic acid chloride **33** to offer the two diastereomers **34** and **35** in quantitative yields (Figure 13). Exploiting the solvent controlled crystallization, effective separation of the *M*-(1*S*)-(+)-TBTQ **35** diastereomer was achieved using toluene, which offered the isomer in 35% yield and excellent de > 99%. On the other hand, the *P*-(1*S*)-(-)-TBTQ **34** diastereomer was recrystallized from $CH_2Cl_2/C_6H_{12}$ to give the isomer in 32% yield and de > 99%. The obtained pure diastereomers were subjected to further transformations, namely hydrolysis of the ester, iodination and finally a Sonogashira-Hagihara coupling reaction without loss of the ee.[52]

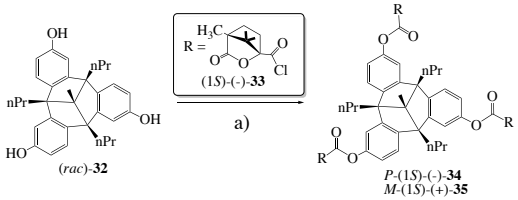


FIGURE 13: Synthesis of *P*-(1*S*)-(-)-TBTQ-**34** and *M*-(1*S*)-(+)-TBTQ-**35** diastereomers. a) (1*S*)-(-)-**33**, DMAP, $NEt_3$, $CH_2Cl_2$, 0° to rt, 19h, 100%.

Racemic mixture of TBTQ trialdehydes, **36** has been optically resolved indirectly by constructing cryptophane derivatives. This approach is identical to that reported above by Warmuth and co-workers. The dynamic covalent assembly of racemic TBTQ-**36** with enantiopure (1*S*,2*S*)-diaminocyclohexane **28** led to the formation of three diastereomeric mixtures of multiple Schiff's bases **37** (Figure 14). The corresponding hydrolysis of these cryptophanes gave rise to the enantiopure *P*-TBTQ-**36**.[53]

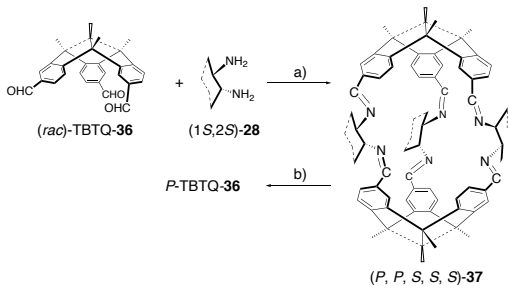


FIGURE 14: Synthesis of *M* and *P*-TBTQ-**36**. a) $CH_2Cl_2$, 29% b) TFA, $CH_2Cl_2$, $H_2O$, 94%.

### *3.2.* Synthesis of cryptophanes from enantiopure CTB derivatives

Enantiopure CTB derivatives are crucial building blocks to prepare optically active cryptophane derivatives. A. Collet and co-workers were the first to develop this approach in order to prepare various optically active cryptophane derivatives. Some examples are discussed below.

Enantiopure anti-**5**, was specifically synthesized to accommodate enantiomerically enriched chlorobromofluoro-methane (CHFClBr).[1] This compound was prepared using a similar approach developed for the synthesis of optically active anti-**1**.[2] Enantiopure *M*-(+)-**16** was alkylated with (4-(2-iodoethoxy)-3-methoxyphenyl)-methanol **38** in a mixture of DMF/HMPA/NaOH to give rise to the desired cryptophane precursor with the M absolute configuration (Figure 15). Cyclisation performed at 95°C offered both the *anti-MM*-**5** and *syn-MP*-**6** derivatives in 20% and 5% yield, respectively. These two diastereomers were easily separated by column chromatography. Despite the relatively high temperature needed to perform the second ring closing reaction, it was observed that the reaction resulted in a moderate decrease of the optical rotation of the cryptophanes suggesting that the cyclisation of the second CTB cap is faster than the crown inversion.

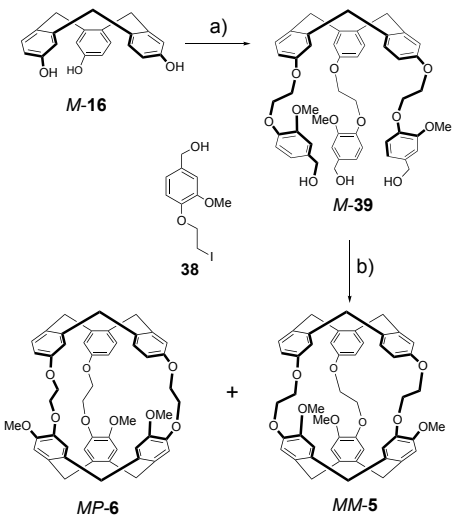

FIGURE 15: synthesis of cryptophane-C (**5**) and D (**6**) from CTB-**16**. A single enantiomer is shown. a) **38**, DMF, HMPA, NaOH, 25°C; 90%. B) HCOOH, 95°C; (*MM*-**5**; 25% and *MP*-**6**; 5%)

Using a similar approach, the CTG **11** has been used to prepare several optically active cryptophane derivatives including *anti*-**1**, or others with longer alkyl chains like cryptophane-E derivative (propylenedioxy linkers).[54] Thus, reacting the *M*-CTG-**11** derivative with (4-(2-bromoethoxy)-3-methoxyphenyl)-methanol-**40** gives rise to the cryptophane precursor *P*-**41** (Figure 16). The second ring closing reaction was performed in formic acid at 50-90°C during a short period to give rise to the corresponding *PP*-**1**. Notably, under these experimental conditions the formation of the *MP*-*syn*-**3** or cryptophane-B was not detected. Similarly, *M*-CTG-**11** was combined with (4-(3-iodopropoxy)-3-methoxyphenyl)-methanol to provide the *PP*-cryptophane-E with high ee.[54] The same chiral CTB derivative allowed the preparation of the optically active *anti*-cryptophane-G derivative bearing three triple bonds.[54] Here again, the relatively high temperature (above room temperature) used to perform the second ring closing reaction decreases the initial ee, which has been estimated to range between 90 and 95 %. Subsequent chemical transformations afforded the enantioenriched cryptophanes decorated with other functionalities.

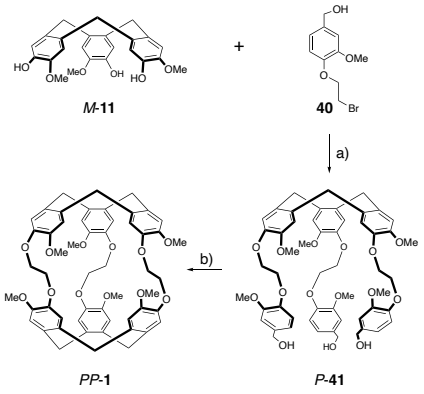


FIGURE 16: Synthesis *PP*-**1** from enantiopure CTB *M*-**11**. a) $Cs_2CO_3$, DMF, 82% b) formic acid, 55-60°C, 80%.

Other cryptophanes bearing ethylenic bridges were also prepared using a similar approach.[55] For instance, the *P*-CTG-**11** enantiomer was employed as a starting material to prepare two ($D_3$/$C_{3h}$) cryptophane pairs of derivatives bearing trans or cis ethylenic bridges in moderate yields. Later, J. Crassous and co-workers used a similar strategy to synthesize enantioenriched sulfur-containing cryptophanes aimed at binding the two enantiomers (*R*) and (*S*) of chlorofluoroiodomethane.[56] In this example, a significant racemization was observed and the two enantiomers *MM* and *PP* of this cryptophane have been obtained with ee of 82 % and 66 %, respectively. Determination of the ee was achieved by chiral HPLC using a Whelk-O1 column. The binding process between the *PP*-enantiomer of this cryptophane and the two enantiomers of CHFClI was assessed by $^{19}F$ and $^{1}H$ NMR spectroscopy. These results show that the preparation of enantiopure cryptophane derivatives from optically active CTB is difficult since a decrease of the enantiomeric excess cannot be avoided during the cyclisation of the second CTB cap. Nevertheless, this approach allows the formation of cryptophane derivatives with high enough ee.

Building multi-dimensional supramolecular structures can be achieved by different methods and coordination driven self-assembly is one of them. A particular interest is given to metallo-cages, which are made up of multi-dentate ligands and metal cations due to their potential applications in catalysis, separation, molecular recognition, and nanoscale vessels.[57] Metallo-cryptophanes constitute an important family of self-assembled CTB and metal cations. These structures may undergo homochiral sorting, ligand exchange or they may exist in coordination networks.[58] For instance, Shinkai and co-workers reported in 2001 the first self-assembled coordination driven cryptophane cage.[59] In this study, a racemic CTB-**42** derivative bearing three pyridyl groups was self-assembled into meso (*syn*-**43**) and chiral (*anti*-**44**) cryptophanes by the coordination with cis-protected palladium salts (Figure 17). Both *anti*-enantiomers were dynamically converted into the *syn*-isomer, which is more thermodynamically stable. Interconversion between these two *syn* and *anti*-structures was observed and fastened by increasing the molar ratio of the racemic ligand with respect to the metal source. The tunable character of these cages is advantageous, as they could change their properties in response to the guest molecule. Enantiopure *M* and *P*-CTB caps have been also obtained from optical resolution on chiral HPLC column (Daicel ChiralcelOD-H) using 1-propanol as the mobile phase. In presence of a square-planar Pd(II) complex, these two optically resolved *M* and *P*-CTB derivatives self-assemble into a chiral cryptophane as the only product.

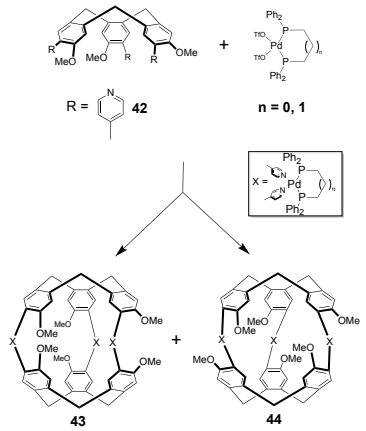


FIGURE 17: Synthesis of Pd-based metallo-cryptophanes.

Another example of enantiopure metallo cryptophanes has been recently reported by Chambron and co-workers.[60] Starting from enantiopure *M* or *P*-CTB$(CN)_3$, which were separated by chiral HPLC on (*S*,*S*)-Whelk-O1 column, enantiopure pallado and platino cryptophanes were obtained using [Pd(dppp)$(OTf)_2$] and [Pt(dppp)$(OTf)_2$] as metal sources. The chiroptical properties of

the two enantiopure metallo-cages were thoroughly investigated by ECD and polarimetry, revealing characteristic properties for each metallo-cryptophane. TD-DFT calculations reproduced the corresponding experimental ECD spectra and provided valuable information about the induced circular dichroism (ICD) from the chiral CTB to the achiral metal bridge. The metallo-cryptophane assembly was further investigated by $^1$H NMR spectroscopy and mass spectrometry. This assembly was found to be stereoselective (only *anti*-cryptophanes were formed) and chemoselective, as the mixing of different CTB derivatives or metals induces a preferential homochiral assembly.

### *3.3.* Synthesis of enantiopure cryptophanes by separation of diastereomers

Since the use of enantioenriched CTB derivatives results in a decrease of the ee of enantiopure cryptophanes, Brotin and co-workers proposed another approach based on the separation of diastereomers of cryptophane derivatives. This approach involved the synthesis of monofunctionalized cryptophane derivatives in their racemic form followed by grafting a chiral substrate to give rise to a couple of diastereomers. In the first example reported in literature, a cryptophane bearing a single phenol group (called cryptophanol) has been prepared from a multi-step synthesis and enantiopure (*S*)-camphanic acid chloride has been used as a chiral subunit.[61] In this study, the two diastereomers displayed large differences of their solubility in toluene. Thus, it was possible to directly obtain a single diastereomer by crystallization in hot toluene. Similarly, the second diastereomer could be obtained by reacting the *rac*-cryptophane with (*R*)-camphanic acid chloride.

Another approach to obtain this second diastereomer relies on recovering the filtrate. Thus, hydrolysis of the filtrate under basic conditions gave rise to the enantioenriched monofunctionalized (+)-cryptophane, which in turn, reacted with the (*R*)-camphanic acid chloride. This allowed the preparation of the second diastereomer in a good yield and diastereomeric excess (de) close to 100%. In this example, the determination of the de has been easily achieved by a direct analysis of $^1$H NMR spectra since the two diastereomers possess distinct $^1$H NMR signature. The synthesis of enantiopure cryptophane derivatives via the formation of diastereomers has several advantages. For instance, once the resolution of the two diastereomers is achieved, the enantiopure *MM* or *PP* monofunctionalized cryptophane derivative can be easily recovered by treatment under basic conditions without any loss of optical purity since the inter-conversion between the cryptophanes is impossible. In addition, thanks to the presence of the reactive phenol function and the production of these two diastereomers in fair quantities, it is now possible to design new enantiopure cryptophanes derivatives without any loss of enantiomeric purities. Thus, using this approach, several enantiopure cryptophane derivatives such as *PP* and *MM*-anti-**1**, *PP* and *MM*-cryptophane-H, *anti*-**45**, *PP* and *MM*-cryptophane-hexahydroxyl, *anti*-**46**, *PP* and *MM*-cryptophane penta-hydroxyl, *anti*-**47**, *PP* and *MM*-cryptophane-hexaacid, *anti*-**48**, have been prepared with ee close to 100% (Figure 18).[61,62]

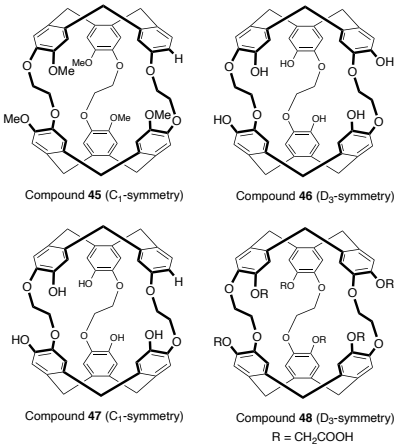


FIGURE 18: Structure of *PP*-(*anti*)-**45**, *PP*-(*anti*)-**46**, *PP*-(*anti*)-**47** and *MM*-(*anti*)-**48**.

Using a similar approach, Dmochowski and co-workers reported the synthesis of cryptophane diastereomers in which a cryptophane bearing three phenol moieties **49** was allowed to react with three (*S*)-Mosher's acid ((*S*)-(-)-α-methoxy-α-trifluoromethylphenylacetic acid **50**) to give two diastereomeric compounds *PM*-(*S*,*S*,*S*)-**51** and *MP*-(*S*,*S*,*S*)-**52** (Figure 19).[63] These two diastereomers were separated by chromatography on silica gel. The removal of the three chiral auxiliaries under basic conditions provided the two tri-hydroxyl cryptophane derivatives without any loss in optical activity. Further functionalization of the two enantiomers resulted in the formation of new cryptophanes. In these examples, the enantiomeric excess was assessed by ECD spectroscopy.

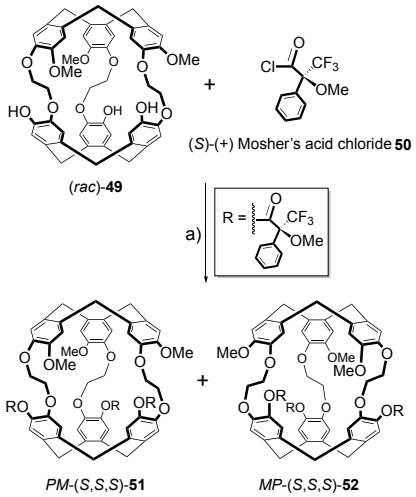


FIGURE 19: Synthesis of cryptophane diastereomers *PM*-(*S*,*S*,*S*)-**51** and *MP*-(*S*,*S*,*S*)-**52**. a) 3.3 equiv. **50**, DMAP, $Et_3N$, reflux. The first letter refers to the stereo-descriptor of the CTB cap located on top.

### 3.4. Separation of enantiomers of cryptophane derivatives by HPLC techniques

Analytical and semi-preparative chiral HPLC are well-known efficient techniques to separate enantiomers of chiral organic compounds such as cryptophane derivatives. These techniques can be used as an analytical tool to determine the enantiomeric excess or to separate enantiomers in order to perform additional characterization using chiroptical techniques. Considerable progress has been made in the field of the enantio-separation by chiral HPLC and chemists today possess stable chiral stationary phases, such as the Chiralpak and Whelk-O1 columns. Thus, it is now possible to isolate fair quantities of enantiopure materials (from several hundreds of mg to gram scale) in a short period of time (2-3 days).

This technique has been used for the first time in 1989 by A. Collet and co-workers for the enantioseparation of CTB (see section 2.2) and cryptophane derivatives.[19] Chiralpak OT(+) was used as the stationary phase to separate chiral cryptophane derivatives exhibiting different symmetry. In the case of cryptophane-E and other cryptophane derivatives having longer bridges, the authors demonstrated that the chiralpak OT(+) column could efficiently separate the three isomers; two enantiomers of *anti*-cryptophane-E ($D_3$-symmetry) and the corresponding achiral syn-cryptophane ($C_{3h}$-symmetry). Later, Crassous and co-workers used the Whelk-O1 column to determine the ee of enantioenriched sulfur-containing cryptophane derivatives.[56]

More recently, Brotin and co-workers used semi-preparative chiral HPLC columns to separate various cryptophane derivatives.[21] Chiralpak columns were especially efficient to separate the two enantiomers of cryptophane derivatives showing large differences in their structures. For instance, four Chiralpak IA, IB, IC and ID HPLC columns have been tested to separate the two enantiomers of *anti*-cryptophane-**2** decorated with twelve methoxy groups, and the two *anti*-**7** and *syn*-**8** bearing nine methoxy groups. In most of these examples, the separation was achieved with very good resolution factors Rs, thus leading to the isolation of each enantiomers with ee $>$ 99.5 % (Table 1). Detection of the enantiomers is usually achieved by coupling a polarimeter or a circular dichroism (CD) detector to the HPLC column. This allows to assign the sign (+) or (-) for the peaks at a given wavelength of detection (usually at 254 nm). It is important to note that this sign can be different from that measured by polarimetry at 589 nm.

Other chiral cryptophane derivatives have been successfully resolved using Chiralpak or (*S*,*S*)-Whelk-O1 columns chromatography. For instance, the two enantiomers of *anti*-**9** and *anti*-**10** have been isolated from a Chiralpak IA column (Table 2).[64] However, these two compounds showed quite low solubility in their racemic forms and large quantities of mobile phase were necessary to isolate the two enantiomers (ee $>$ 99.5 %) of *anti*-**9** and *anti*-**10** in fair quantities. Once isolated, each enantiomer of compounds **9** and **10** has been recrystallized from a $CHCl_3$/EtOH mixture.

Chiral HPLC was used with confidence to separate the two enantiomers of cryptophane-222, *anti*-**53**, and cryptophane-111, *anti*-**54**, with excellent ee.[65,66] It is noteworthy that both compounds **53** and **54** are devoid of substituents (Figure 20). Thus, an approach based on the separation of diastereomers is not possible in this case. The two enantiomers of *anti*-**53** and *anti*-**54** were isolated from a Chiralpak-ID semi-preparative column (Table 2) with excellent resolution factors Rs = 2.36 and Rs = 3.24, respectively. For these two examples, it is remarkable that HPLC columns can discriminate the two enantiomers of these two derivatives considering their globular shapes.

Several cryptophane derivatives having $C_1$-symmetry were also successfully separated by chiral chromatography techniques. For instance, the two enantiomers of a cryptophane-223, *anti*-**55**, bearing an allyl moiety grafted on the propylenedioxy linker were separated with an excellent resolution factor (Rs = 5.04) and with excellent ee $>$ 99.5 % using a Chiralpak ID column.[67] Other enantiopure cryptophane-223 derivatives (compounds **56**-**58**) decorated with acetate moieties were isolated with high ee using Chiralpak IC or (*S*,*S*)-Whelk-O1 HPLC semi-preparative columns (Table 2).[68]

TABLE 1: Separation of the two enantiomers of compounds *anti*-cryptophane-**2**, *anti*-cryptophane-**7** and *syn*-cryptophane-**8** performed at 25°C by using analytical chiral stationary phases (250 x 4.6 mm). The name of the chiral column is reported and the experimental conditions (mobile phase) are given. $t_1$ and $t_2$ are the retention times (min) of the two enantiomers. $k_1$ and $k_2$ are the retention factors, $\alpha$ is the enantioselectivity factor and $R_s$ is the resolution factor. (+) and (-) refer to the sign measured at 254 nm by using a polarimeter or a circular dichroism detector.

| Column | Mobile Phase | $t_1$ | $k_1$ | $t_2$ | $k_2$ | $\alpha$ | $R_s$ |
|---|---|---|---|---|---|---|---|
| | *anti*-**2** [21] | | | | | | |
| Chiralpak IC | Hexane/EtOH/$CHCl_3$ 50/30/20 | 4.02 (-) | 0.34 | 4.47 (+) | 0.49 | 1.44 | 1.07 |
| | Hexane/2-PrOH/$CHCl_3$ 50/30/20 | 4.18 (-) | 0.39 | 5.71 (+) | 0.9 | 2.3 | 2.17 |
| Chiralpak ID | Hexane/EtOH/$CHCl_3$ 50/30/20 | 5.15 (+) | 0.72 | 7.18 (-) | 1.39 | 1.95 | 4.88 |
| | Hexane/2-PrOH/$CHCl_3$ 50/30/20 | 4.54 (+) | 0.51 | 6.07 (-) | 1.02 | 2.00 | 3.97 |
| | *anti*-**7** [21] | | | | | | |
| Chiralpak IA | Hexane/EtOH/$CHCl_3$ 50/30/20 | 7.80 (+) | 1.60 | 8.61 (-) | 1.87 | 1.17 | 1.48 |
| | Hexane/2-PrOH/$CHCl_3$ 50/30/20 | 4.70 (+) | 0.57 | 5.37 (-) | 0.79 | 1.40 | 1.94 |
| Chiralpak IB | Hexane/EtOH/$CHCl_3$ 50/30/20 | 4.97 (+) | 0.66 | 6.81 (-) | 1.27 | 1.94 | 3.58 |
| | Hexane/2-PrOH/$CHCl_3$ 50/30/20 | 5.49 (+) | 0.83 | 9.51 (-) | 2.17 | 2.62 | 5.90 |
| Chiralpak IC | Hexane/EtOH/$CHCl_3$ 50/30/20 | 7.59 (+) | 1.53 | 9.51 (-) | 2.17 | 2.62 | 5.90 |
| | Hexane/2-PrOH/$CHCl_3$ 50/30/20 | 9.73 (+) | 2.24 | > 45 min | | | |
| Chiralpak ID | Hexane/EtOH/$CHCl_3$ 50/30/20 | 28.93 (-) | 8.64 | - | - | 1 | - |
| | Hexane/2-PrOH/$CHCl_3$ 50/30/20 | 21.17 (-) | 6.06 | 25.10 (+) | 7.37 | 1.22 | 1.52 |
| | *syn*-**8** [21] | | | | | | |
| Chiralpak IA | Hexane/EtOH/$CHCl_3$ 50/30/20 | 6.79 (-) | 1.26 | 10.70 (+) | 2.57 | 2.03 | 6.37 |
| | Hexane/2-PrOH/$CHCl_3$ 50/30/20 | 5.21 (-) | 0.74 | 6.15 (+) | 1.05 | 1.43 | 2.38 |
| Chiralpak IB | Hexane/EtOH/$CHCl_3$ 50/30/20 | 5.01 | 0.67 | / | / | 1 | 0 |
| | Hexane/2-PrOH/$CHCl_3$ 50/30/20 | 5.43 (+) | 0.81 | 5.87 (-) | 0.96 | 1.18 | 0.73 |
| Chiralpak IC | Hexane/EtOH/$CHCl_3$ 50/30/20 | 9.60 (+) | 2.20 | 11.51 (-) | 2.84 | 1.29 | 1.29 |
| | Hexane/2-PrOH/$CHCl_3$ 50/30/20 | 11.10 (+) | 2.70 | 20.01 (-) | 5.67 | 2.10 | 2.91 |
| Chiralpak ID | Hexane/EtOH/$CHCl_3$ 50/30/20 | 17.20 (-) | 4.73 | 28.78 (+) | 8.59 | 1.82 | 5.58 |
| | Hexane/2-PrOH/$CHCl_3$ 50/30/20 | 14.67 (-) | 3.89 | 34.45 (+) | 10.48 | 2.69 | 5.94 |

TABLE 2: Separation of the two enantiomers of compounds **9**-**10** and **53**-**58** performed at 25°C by using analytical chiral stationary phases (250 x 4.6 mm). The name of the chiral column is reported and the experimental conditions (mobile phase) are given. $t_1$ and $t_2$ are the retention times (min) of the two enantiomers, $k_1$ and $k_2$ are the retention factors, $\alpha$ is the enantioselectivity factor and $R_s$ is the resolution factor. (+) and (-) refer to the sign measured at 254 nm by using a polarimeter or a circular dichroism detector.

| Column | Mobile Phase | $t_1$ | $k_1$ | $t_2$ | $k_2$ | $\alpha$ | $R_s$ |
|---|---|---|---|---|---|---|---|
| | Compound **9** [64] | | | | | | |
| Chiralpak IA | Hexane/EtOH/$CHCl_3$ 20/40/40 | 5.45 (+) | 0.82 | 8.41 (-) | 1.80 | 2.21 | 4.19 |
| | Compound **10** [64] | | | | | | |
| Chiralpak IA | Hexane/EtOH/$CHCl_3$ 20/40/40 | 7.48 (+) | 1.49 | 15.73 (-) | 4.24 | 2.84 | 4.02 |
| | Compound **53** [65] | | | | | | |
| Chiralpak IB | Heptane/EtOH/$CHCl_3$ 20/40/40 | 4.54 (-) | 0.51 | 5.39 (+) | 0.80 | 1.56 | 2.36 |
| | Compound **54** [66] | | | | | | |
| Chiralpak ID | Heptane/EtOH/$CHCl_3$ 50/30/20 | 6.95 (-) | 1.32 | 9.03 (+) | 2.01 | 1.52 | 3.24 |
| | Compound **55** [67] | | | | | | |
| Chiralpak ID | EtOH/$CH_2Cl_2$ 20/80 | 3.84 (-) | 0.28 | 5.33 (+) | 0.78 | 2.79 | 5.04 |
| | Compound **56** [67] | | | | | | |
| Chiralpak IC | Heptane/EtOH/$CH_2Cl_2$ 50/10/40 | 4.89 (-) | 0.63 | 6.48 (+) | 1.16 | 1.84 | 2.23 |
| | Compound **57** [68] | | | | | | |
| (*S*,*S*)-Whelk-O1 | Heptane/EtOH/$CH_2Cl_2$ 20/40/40 | 9.13 (-) | 2.10 | 12.7 (+) | 3.29 | 1.57 | 5.72 |
| | Compound **58** [68] | | | | | | |
| (*S*,*S*)-Whelk-O1 | EtOH/$CH_2Cl_2$ 50/50 | 5.30 (-) | 0.80 | 6.86 (+) | 1.32 | 1.67 | 4.81 |

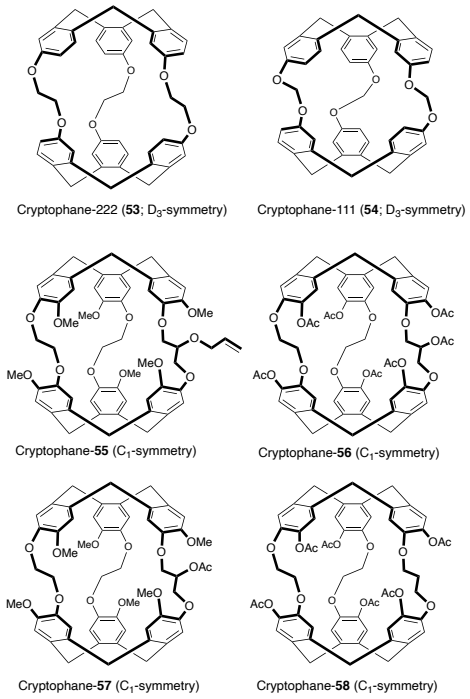


FIGURE 20: Structures of cryptophane derivatives **53**-**58** resolved by chiral HPLC columns.

### *4.* Chiroptical Properties of Enantiopure Cryptophanes [69]

Chiroptical techniques, such as polarimetry, ECD, VCD and ROA spectroscopy, are valuable tools for studying enantiopure cryptophane derivatives and their complexes. The principal uses of these techniques remains the determination of the absolute configuration (AC) of chiral compounds in solution. These spectroscopic techniques also afford useful insights on how the presence of a solvent or any guest molecule within the cavity affects the conformation of the linkers.

#### *4.1.* Determination of the absolute configuration of cryptophane derivatives

The determination of the AC of cryptophane derivatives can be done in the same way as for CTB derivatives, using exciton coupling between identical chromophores. Indeed, the correct assignment of the AC of the CTB derivatives was performed in the light of a coupled-oscillator model, which allows an easy interpretation of the ECD spectra of CTB derivatives of $C_3$-symmetry for the two forbidden electronic transition $^1L_a$ ($^1B_{1u}$) and $^1L_b$ ($^1B_{2u}$) bands (Platt's notation) located at high wavelengths (240-310 nm).[70] This model is an extension of the famous two-coupled oscillator model described by Harada and Nakanishi, which has been widely used by chemists for the determination of the AC of organic molecules.[71,72]

In the example reported in Figure 21, let's consider an optically active CTB derivative ($X \neq Y$) with $C_3$-symmetry and let's consider only the lowest excited state ($^1L_b$) for benzene rings. The three electronic transitions moments of each benzene ring interact with each other to give rise to three new excited states (one A and two degenerate E components). Due to symmetry consideration, the overall electronic transition moment **μ** and magnetic moment **m** are parallel (positive rotational strength) for the A excited state and anti-parallel (negative rotational strength) for the two E excited states (Figure 21a). The ability of the substituents to tilt, by an angle θ, the electronic transition moments of the $^1L_b$ transitions determine the sign and position of each A and E components on the ECD spectrum. For $C_3$-symmetrical CTB derivatives, four specific regions (I, II, III, IV) have been identified, corresponding to deviation angle θ ~ 0-45°, 45-90°, 90-135°, and 135-180°, where the ECD excitonic pattern is inverted (Figure 21b). The spectroscopic moment of the substituents X and Y determine the sign and the magnitude of the deviation angle at which the $^1L_b$ transition is tilted. Spectroscopic moments are parameters that have been introduced to quantify the effect of substituents on the intensity of electronic transitions. The same reasoning can of course be extended to the Cotton bands of $^1L_a$ transition for which the angle θ is roughly perpendicular to the one of $^1L_b$ transition. Thus, the rapid assignment of the stereo-descriptor M or P for $C_3$-symmetrical CTB derivatives can be deduced from the analysis of their ECD spectra.[30]

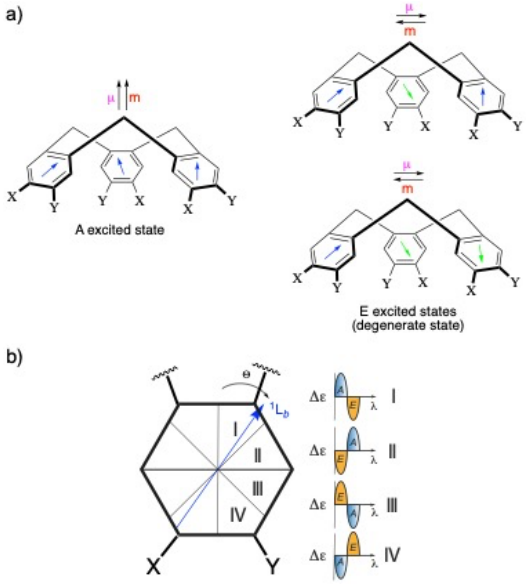


FIGURE 21: a) Schematic representation of the A and E components resulting from the excitonic coupling between the three $^1L_b$ transitions (blue and green arrows). b) Dependence of the ECD spectrum for the $^1L_b$ transition as a function of the angle θ (here, Y has a larger spectroscopic moment than X). Reproduced from Ref. 3 with permission from Elsevier.

A similar approach can be used for the determination of AC of cryptophane derivatives. However, the interpretation of their ECD spectra appears to be more complicated because the coupled-oscillator model involves six chromophores interacting with each other instead of three for the CTB derivatives. Nevertheless, Collet and Gotarelli proposed an interpretation of ECD spectra of $D_3$-symmetry cryptophanes based on the formalism of group theory.[54] Thus, they showed that each electronic transition $^1L_a$ and $^1L_b$ decompose into three excited states (two E components of opposite sign close in energy and one $A_2$ component). The analysis of six cryptophane derivatives decorated with different substituents (OH, $OCH_3$, $OCOCH_3$, $OCH_2COOCH_3$) reveals the reliability of this model and allows the prediction of the ECD spectra with a good degree of confidence. However, few parameters such as temperature, solvent, guest inclusion can affect the shape of the ECD spectra of cryptophanes, In addition, cryptophane derivatives show high flexibility and different conformers can coexist in solution.

Conventional ECD spectrometer usually records ECD spectra between 350 and 200 nm. However, this spectral range can be extended up to 170 nm using Synchrotron Radiation Circular Dichroism Spectroscopy (SRCD). This allows the identification of new Cotton bands ($^1B_b$ region) that can be useful to interpret the behavior of these compounds in solution.[65,66] SRCD requires higher concentration and smaller path-lengths than conventional ECD spectroscopy.

Numerous cryptophane derivatives have been studied by ECD spectroscopy and the analysis of their spectra suggests that it is possible to assign with confidence the correct AC of cryptophane derivatives without using quantum calculations. Indeed, analysis of the ECD spectra of many cryptophane derivatives reveals that, unlike the Cotton bands associated with $^1L_b$ transitions, the Cotton bands located at lower wavelengths (typically 240-260 nm) and associated with $^1L_a$ electronic transitions are generally less sensitive to parameters such as the nature of the linkers, the symmetry of the host, and even the nature of the substituents grafted onto the benzene rings. These Cotton bands commonly appear as a dissymetrical positive-negative or negative–positive bisignate depending on the AC of the cryptophane studied. Thus, the AC of a large range of enantiopure cryptophane can be simply and rapidly determined by this means. Taking as a reference the ECD spectrum of a cryptophane whose AC is known, for instance the *MM*-(-)-**1**, the assignment of the AC of several cryptophane derivatives can be rapidly obtained by comparison (Figure 22). The ECD spectrum of the *MM*-(-)-**1** enantiomer reveals a (+,-)-bisignate from low to high wavelengths (230-260 nm). Similar patterns were also observed in the same region for compounds *anti*-(-)-**2**, *anti*-(-)-**7** and *anti*-(-)-**45**.[21,62] The *anti*-(-)-cryptophane-E that has three propylenedioxy linkers instead of ethylenedioxy linkers shows similar features in its ECD spectrum. The similarities observed between these spectra in the $^1L_a$ spectral region ascertain that these different compounds possess the same spatial arrangement of substituents, thus facilitating the determination of their AC by comparison. In all the examples reported, the use of additional techniques such as VCD or ROA spectroscopy has confirmed these results.

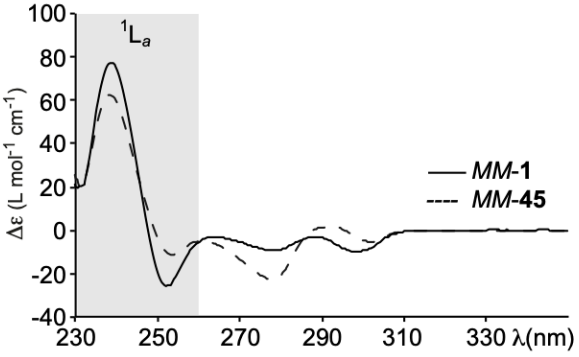


FIGURE 22: ECD spectra of cryptophanes *MM*-**1** and *MM*-**45**.

The approach reported above is based on a comparison of experimental ECD spectra of cryptophane whose AC is unknown with a compound of reference. This approach is convenient, rapid and efficient when measurements are performed in organic solvents ($CHCl_3$, Dioxane). In aqueous solvents, some recent results suggest that the situation can be different. For instance, cryptophane derivatives bearing ionizable substituents such as compounds **46**-**47** have been widely studied by Brotin and co-workers.[73] The study of their ECD spectra reveals that their shape strongly depends on the nature of the basic solution and its concentration. Similarly, the presence or the absence of a guest molecule in the host cavity modifies significantly the shape of the ECD spectrum. Consequently, the approach reported above does not apply for these two derivatives and the AC cannot be simply determined by ECD spectroscopy.

The AC of new cryptophane derivatives with uncommon structures is more complicated to be assured by this approach. For instance, compounds *anti*-**9** ($C_2$-symmetry) and *anti*-**54** ($D_3$-symmetry) do not exhibit the classical bisignate observed in the $^1L_a$ spectral region. Instead, a single positive or a negative band is present in this region, depending on the enantiomer studied. This feature makes the rapid assignment of their AC by ECD spectroscopy more difficult. In the case of the *anti*-**54**, TD-DFT calculations have revealed that the $A_2$ component (excited state) that appears at high wavelength possesses low negative rotational strength. This excited state is embedded by the two E components that show higher rotational strengths. Consequently, the classical bisignate is replaced by a single positive broad band for *MM*-(+)-**54** in $CHCl_3$.[65]

When the direct assignment of AC of cryptophanes by the bisignate pattern of the $^1L_a$ band is not possible, TD-DFT calculations can be used to determine the AC of enantiopure cryptophanes. This approach is more rigorous and it requires additional skills (quantum calculation) along with computing facilities. Prediction of ECD spectra of cryptophane derivatives has been achieved for compounds having different symmetries such as *anti*-**1**, *anti*-**9**, *anti*-**10** and *anti*-**54**. The use of TD-DFT calculations can be time consuming considering the large number of atoms that composes the cryptophane skeleton. Other parameters such as the basis set and the functional used to

perform these calculations have a strong impact on the computational time needed to reproduce the experimental spectrum. Unlike VCD spectroscopy, which only considers the fundamental state, the prediction of ECD spectra must take into account a large number of excited states in order to obtain reliable results. Thus, the wider the spectral range we want to reproduce, the greater the number of excited states to be considered. In addition, since several conformers can be present in solution, a conformational search is necessary. Unfortunately, this conformational search can only be carried out for cryptophane derivatives with short linkers (methylenedioxy or ethylenedioxy), because the number of combinations increases significantly as the length of the bridges increases. However, when the conformational search is expected to be time-demanding, some assumptions can be made. For instance, guest molecule with a large molecular volume will mainly favour the trans-trans-trans (*ttt*) or gauche-trans-trans (*gtt*) conformations of the linkers. In contrast, small guest molecules or guest free cryptophane derivatives will favour the gauche-gauche-gauche (*ggg*) conformation of the linkers in order to reduce the cavity size of the host.

A geometry optimization of the cryptophane is usually performed at the DFT level. Generally, B3PW91 functional and basis set 6-31G** have been used for geometry optimization of cryptophane derivatives. If available, an X-ray crystal structure can be used as the starting point of the geometry optimization. In a second step, the UV-Visible spectra (excitation energies and associated oscillator strengths) and ECD spectra (excitation energies and rotational strengths) are calculated using TD-DFT. Herein, the choice of the functional and basis set is crucial. For the prediction of the ECD spectra of cryptophane derivatives, the use of CAM-B3LYP or MPW1K (containing 42.8% of HF exchange) functionals and the 6-31+G** basis set is recommended to have reliable results. In order to take into account solvent molecules, a polarizable continuum model can be included in the calculation. Predicted ECD spectra are often shifted towards low wavelength with respect to the experimental spectrum. Usually, predicted ECD spectra reproduce fairly well the experimental ones, as shown in Figure 23 with the ECD spectrum of $CHCl_3$@*PP*-**1** complex assuming a *gtt* conformation of the linkers.[21] Although it is difficult to obtain reliable information on the conformation of the linkers for cryptophane derivatives in solution, the combined use of ECD spectroscopy and TD-DFT calculations provides a convenient method for determining the AC of these compounds.

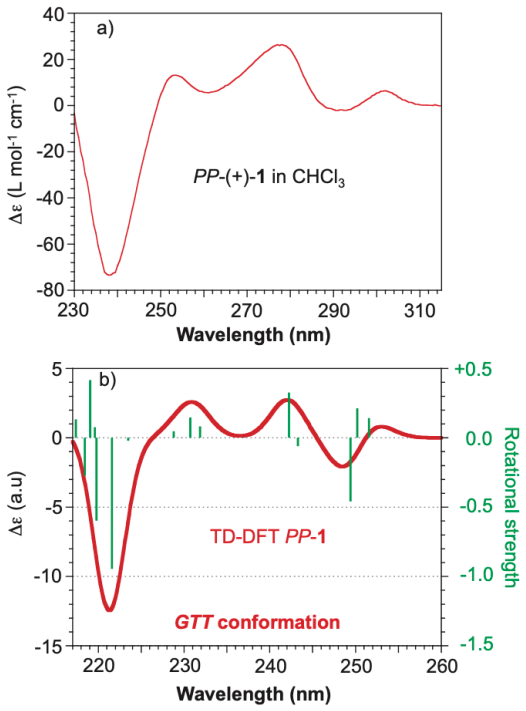


FIGURE 23: a) Experimental ECD spectrum of (+)-**1** in $CHCl_3$ solution and b) calculated ECD spectrum of *PP*-**1** by TD-DFT, assuming a *gtt* conformation for the three ethylenedioxy linkers. The rotational strengths (blue bars) should be multiplied by $10^{-40}$ erg.esu.cm/Gauss. Adapted with permission from ref. 21. (2014) American Chemical Society.

Vibrational Optical Activity (VOA) techniques such as Vibrational Circular Dichroism (VCD) and Raman Optical Activity (ROA) are other important chiroptical techniques, which have been used to determine the AC of cryptophane derivatives. Comparison of the VCD and ROA spectra to the predicted spectra by DFT calculations offers an efficient tool to assign the AC and the conformation of cryptophane derivatives. Similar to ECD spectra calculations, a conformational search is performed to predict VCD spectra as several conformers close in energy may contribute significantly to the overall VCD spectrum. Usually, only conformers in the range of 5 kcal $mol^{-1}$ from the lowest energy conformer are selected for geometry optimization. Geometry optimization is usually performed at the DFT level by using B3PW91 or B3LYP functionals and 6-31G* or 6-31G** basis sets. Vibrational frequencies, IR and VCD intensities are then calculated at the same level of theory. For comparison to experiments, the calculated frequencies are scaled by 0.968 and the calculated intensities are converted to Lorentzian bands with half-width of 7 $cm^{-1}$.

VCD spectroscopy and DFT calculations were used to ascertain the AC of the two enantiomers of *anti*-**1**.[74] VCD spectra showing a perfect mirror image have been obtained for the two enantiomers of **1** between 3150-2750 $cm^{-1}$ (C-H stretching region) and the 1700-1000 $cm^{-1}$ spectral region in $CDCl_3$. The combined use of DFT calculations and VCD spectroscopy allowed for the

first time the direct determination of the AC of a cryptophane derivative. Calculations were performed at the DFT level using various functional and basis set, allowing the assignment of the AC of the two enantiomers with high confidence. It is noteworthy that the low basis set such as 3-21G* appears to be sufficient to determine the AC (Figure 24a). The results obtained by VCD spectroscopy were consistent with those previously obtained by ECD spectroscopy. In addition, these results made it possible to establish the preferential *ttt* conformation for the three linkers of $CHCl_3$@**1** complex (Figure 24b). It was observed that a change in the nature of the solvent does not affect significantly the global shape of the VCD spectra. Indeed, similar VCD spectra were obtained in tetrachloroethane-$d_2$ (guest-free cryptophane) and in $CDCl_3$ or $CD_2Cl_2$ solvent (encaged solvents). Independently, Raghavachari and co-workers were able to reproduce the VCD spectrum of the *anti*-**1** derivative using a novel approach based on the Molecules-in-Molecules (MIM) fragment-based method.[75] This method seems particularly well adapted to rapidly predict VCD spectra of large molecules such as cryptophane derivatives. More recently, Weigend and co-workers reported in 2017 a simulation of the VCD spectrum of *anti*-**1** derivative using various functionals and basis sets.[76] The authors studied the impact of these setting on the quality of the VCD spectra and the computational times required to obtain the results.

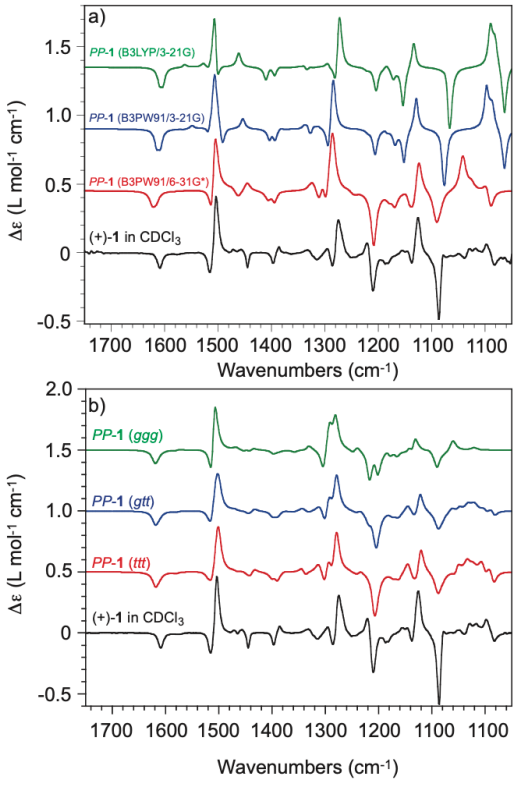


FIGURE 24: a) Comparison of experimental VCD spectrum of (+)-**1** recorded in $CDCl_3$ solution with calculated spectra for the *ttt* conformer of *PP*-**1** at the B3LYP/3-21G, B3PW91/3-21G and B3PW91/6-31G* levels. b) Comparison of experimental VCD spectrum of (+)-**1** recorded in $CDCl_3$ solution with calculated spectra at the B3PW91/6-31G** level for *ttt*, *gtt* and *ggg* conformers of $CHCl_3$@*PP*-**1** complex. Adapted with permission from ref. 74. (2006) American Chemical Society.

Since then, VCD spectra of several cryptophane derivatives having different symmetries and substituents have been measured. For instance, $C_1$-symmetry compound such as **45** has been studied by VCD spectroscopy in three solvents ($CDCl_3$ and $CD_2Cl_2$, two solvents that can enter the cavity of the host and $C_2D_2Cl_4$ a too large solvent to enter the cavity of the host) and their spectra were predicted by DFT calculations.[77] Calculations were performed at the DFT level using B3PW91 functional and 6-31G* basis set, considering different conformations of the linkers (*ggg*, *gtt* and *ttt*). A chloroform molecule was inserted into the cavity of the host molecule to predict the VCD spectrum of **45** in $CDCl_3$, whereas the empty cryptophane was considered to predict the VCD spectrum of **45** in $C_2D_2Cl_4$. The predicted VCD spectra reproduced very well the VCD spectra recorded in the three solvents, allowing the unambiguous determination of the AC of this compound. Information was also obtained concerning the conformers present in solution. For instance, it was observed that the guest-free cryptophane in $C_2D_2Cl_4$ shows a preferential *ggg* conformation of the three linkers. In contrast, the calculation revealed that the $CHCl_3$@**45** complex shows a preferential *gtt* conformation of the linkers. Similarly, using an equivalent approach, the AC of *anti*-**9** and *anti*-**10** were easily determined by this technique.[64] These two compounds showed VCD spectra similar to that of *anti*-**1** even though the intensities of some VCD bands were found to be smaller. It is noteworthy that, in these examples, a conformational search would be extremely time consuming considering the large number of conformers possible. Thus, DFT calculations were performed assuming a single conformation of the linkers. This assumption was sufficient to ascertain the AC of these derivatives.

The VCD spectra of *anti*-**2** and *anti*-**7** as well as the VCD spectrum of the syn-**8** have also been reported and compared to that of the *anti*-**1** derivative.[21] Very different VCD spectra have been measured for these three cryptophanes in $CDCl_3$. The spectral differences are even more pronounced for the syn-**8** derivative whose VCD spectrum exhibits vibrational transitions of lower intensities than its congeners. The combined use of VCD and DFT (B3PW91/6-31G** level) calculations allowed to assign the *PP*-(+) absolute configuration for compounds *anti*-**7** and *anti*-**2**. A comparison between the experimental and theoretical VCD spectra revealed the preferential *gtt* conformation of the linkers for these two compounds. Moreover, the *PM*-(+) absolute configuration has been assigned for *syn*-**8**. For this compound, the DFT calculation did not show a good correlation between the experimental and theoretical spectra, and the conformation adopted by the three linkers was considered trickier.

In another study, it was observed that the VCD spectrum of *anti*-**53** is quite different from that of *anti*-**1**.[66] The lack of substituents on *anti*-**53** drastically affects the intensities and frequencies of the vibrational transitions. A comparison between both the experimental and theoretical (B3PW91/6-31G** DFT level) spectra allowed to assign the *PP*-(-) absolute configuration for

compound *anti*-**53**. This assignment was confirmed independently by ECD spectroscopy and X-ray crystallography. It is worth mentioning that compound *anti*-**53** shows SOR values very different from those measured for *anti*-**1**. Indeed, the SOR values of *anti*-**53** are lower than those measured for *anti*-**1**, whatever the wavelength and the solvent used. The higher flexibility of compound *anti*-**53** seems to be responsible of this effect. *Anti*-**54** possesses identical CTB caps than compound **53** but with shorter linkers. As a result, the cavity of *anti*-**54** is smaller and it cannot accommodate small solvent molecules such as $CH_2Cl_2$. The number of conformations adopted by the linkers is also significantly reduced compared to other derivatives bearing ethylenedioxy bridges. Consequently, the VCD spectra recorded in $CDCl_3$ and $CD_2Cl_2$ were found superimposable.[65] This structural simplification facilitates the use of DFT calculations and a very good agreement was observed between the theoretical and the experimental spectra. Thus, the *MM*-(+) absolute configuration was assigned for compound *anti*-**54**. This assignment was also confirmed by ECD spectroscopy and X-ray crystallography.

Raman Optical Activity (ROA) can also be used to characterize optically active cryptophane derivatives. As for VCD spectroscopy, the comparison between theoretical and experimental ROA spectra permits the determination of the AC of cryptophane derivatives. In addition, useful information on the conformation of the linkers can be obtained by this technique. Interestingly, ROA spectra cover a large spectroscopic range (from 2000 $cm^{-1}$ up to 100 $cm^{-1}$). Thus, ROA spectroscopy appears as a complementary tool to VCD spectroscopy as it gives access to vibrational modes that cannot be detected by VCD spectroscopy.

*Anti*-**1** and its congeners *anti*-**2**, *anti*-**7** and *syn*-**8** have been studied by ROA spectroscopy.[78] A comparison between the experimental and the theoretical (B3PW91/6-31G** DFT level) spectra allows to establish the AC of these derivatives. These AC were found in perfect agreement with those measured by VCD spectroscopy or other chiroptical techniques. In addition, as previously observed by VCD spectroscopy, the preferential *ttt* conformation for the linkers has been predicted for *anti*-**1**, *anti*-**2** and *anti*-**7**. It is noteworthy that the ROA spectrum of compound **7** (bearing nine methoxy substituents) are almost half the sum of the ROA spectra of compounds **1** (bearing six methoxy substituents) and **2** (bearing twelve methoxy substituents), as shown in Figure 25a. This feature indicates that the spectral modifications in Figure 25a come from the difference in the CTV scaffolds rather than a conformational modification of the linkers. In addition, completely different ROA spectra were measured for *anti*-**7** and *syn*-**8** (Figure 25b). Thus, this study has revealed that the number of the methoxy substituents and the arrangement (*anti* or *syn*) of the linkers are two parameters which strongly affect the ROA spectra. In contrast, the comparison between ROA spectra of *anti*-**1** and *anti*-**45** shows that a change in molecular symmetry has little impact on the ROA spectra. On the other hand, Raghavachari and co-workers were able to use their theoretical approach (MIM) fragment-based method to reproduce the ROA spectrum of compound 1.[79]

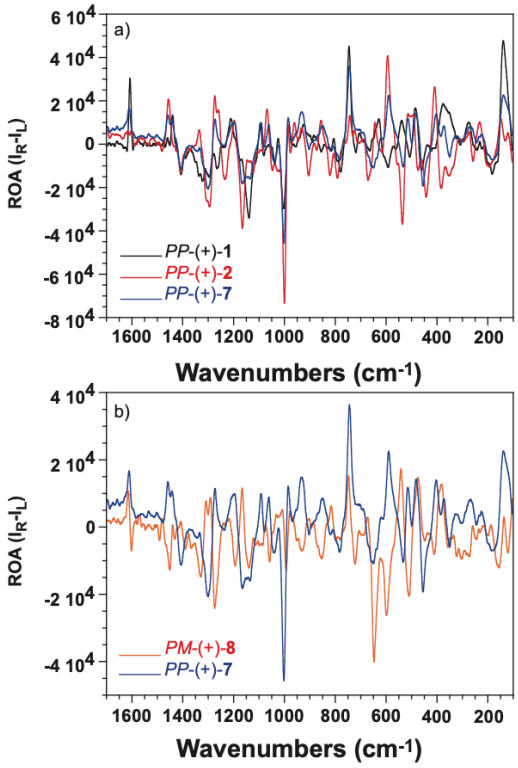


FIGURE 25: a) Comparison of ROA spectra of (+)-*anti*-**1**, (+)-*anti*-**2** and (+)-*anti*-**7** recorded at 295 K in $CDCl_3$ solution (0.1 M). b) Comparison of ROA spectra of (+)-*anti*-**7** and (+)-*syn*-**8** recorded at 295 K in $CDCl_3$ solution (0.1 M). ). Adapted with permission from Ref. 78. (2014) American Chemical Society.

Similar ROA spectra have been measured in $CDCl_3$ for cryptophanes *anti*-**9** and *anti*-**10**.[64] The two enantiomers of compound *anti*-**54** have also been studied by ROA spectroscopy, revealing vibrational transitions with higher intensity (in particular in the 800-400 $cm^{-1}$ spectral region) compared to the other cryptophanes.[65] It is interesting to note that a change in the nature of the solvent does not affect the ROA spectra. This is consistent with the fact that neither $CD_2Cl_2$ nor $CDCl_3$ can enter the cavity of host **54** and modify the conformation of the linkers.

X-ray crystallography is also a reliable method to determine the AC of cryptophane derivatives. However, to date this technique has only been applied to few derivatives. The preparation of good quality crystals is a first prerequisite for obtaining X-ray crystallographic structures but this step can be tedious for cryptophane derivatives. Despite the fact that the overwhelming majority of cryptophane does not contain atoms heavier than oxygen, the Flack parameter can be determined with confidence to attribute the AC of these compounds. For instance, good quality X-ray crystals have been obtained for the two enantiomers of *anti*-**9** and *anti*-**10** in a $CHCl_3$/EtOH mixture.[64] The two enantiomers of *anti*-**9** crystallize in a $P2_1$ space group and those of *anti*-**10** crystallize in a $P3_2$ space group. For these four derivatives, the Flack parameter was measured to be close to 0 as expected for enantiopure derivatives, thus allowing the AC of these derivatives

to be assigned very easily. Similarly, the AC of the two enantiomers of *anti*-**53** was also assigned by X-ray crystallography and was found in good agreement with the AC determined in solution by other chiroptical techniques.[66] It is worth mentioning that the X-ray structures provide additional information on the conformation of the linkers in the solid state. Thus, X-ray crystallography appears to be a useful tool to detect whether several conformers are present in the crystal structure. The presence of several conformers is usually characterized by some disorder in the linkers. This information can thus be exploited to select one or several conformers for DFT calculation. However, it is important to keep in mind that the preferential conformer found in the crystal lattice does not necessarily represent the one found in solution as the crystal packing can modify the relative population of conformers. This effect was nicely exemplified by studying the two enantiomers of *anti*-**54**. The two enantiomers of this compound were obtained in two different solvents and their AC has been unambiguously determined thanks to the determination of the Flack and Hooft parameters.[65] Thus, good quality X-ray crystals of the enantiomer *PP*-**54** were obtained in $CH_2Cl_2$/EtOH, which crystallizes in a $P2_12_12_1$ space group (Figure 26, right). On the other hand, X-ray crystals of the enantiomer *MM*-**54** were obtained in pyridine, which crystallizes in a $P2_1$ space group (Figure 26, left). Interestingly, the conformers observed in the structure of *MM*-**54** and *PP*-**54** do not allow the accurate reproduction of the experimental VCD spectrum. In contrast, a minimized structure obtained from the X-ray crystallographic structure of rac-**54** shows a different conformation of the three methylenedioxy linkers, allowing a quite well VCD prediction of enantiomers *MM*-**54** and *PP*-**54**.

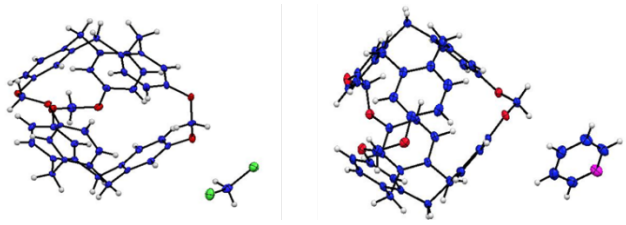

FIGURE 26: X-ray crystallographic structure of *MM*-**54** (left: solvent of crystallization $CH_2Cl_2$) and *PP*-**54** (right: solvent of crystallization pyridine). Flack parameter is F = -0.031 for *MM*-**54** and F = -0.041 for *PP*-**54**. Reproduced from Ref. 65 with permission from The Royal Society of Chemistry.

NMR spectroscopy is another powerful tool that has been extensively used for the determination the AC of organic compounds.[80,81,82] This technique requires the use of chiral derivatizing reagents that can establish specific interactions with the molecule of interest. Up to now, this technique has never been applied to determine the AC of cryptophanes probably due to the difficulties to find the appropriate chiral derivatizing reagent and the good experimental conditions (concentration, solvent). In this concern, only two examples have been reported in the literature between cryptophane and chiral species. Bartik and co-workers reported the $^{129}$Xe NMR spectrum of the Xe@(*rac*)-*anti*-**1** complex in tetrachloroethane-$d_2$ in presence of a chiral europium derivative.[83] Thus, the $^{129}$Xe NMR spectrum, initially composed of a single peak for the xenon-complex, splits into two signals of different widths when the cryptophane is placed with an excess of (tris[3-(heptafluoropropyl-hydroxymethylene-d-camphorato]-europium (III). On the other hand, Duddeck and co-workers reported $^1$H and $^{13}$C NMR spectra for several CTB and cryptophane derivatives in presence of an equimolar amount of $Rh_2$[(*R*)-(+)-MTPA].[84] They showed that in all cases a good enantiodifferenciation takes place thus allowing the rapid determination of the ee by this method.

In conclusion, chemists have now in hand several spectroscopic tools to determine with confidence the AC of cryptophanes. Even though, to date, VCD remains the technique of choice to assign the stereo-descriptors of enantiopure cryptophanes, it is usually recommended to use several chiroptical techniques to assign the AC of organic molecules.[85,86,87]

## *5.* Chiroptical Properties of Cryptophane Complexes

In this section, the chiroptical properties of several cryptophane complexes are presented along with the information regarding the binding of different guests. These complexes have been studied by different chiroptical techniques (ECD, VCD and ROA) combined with DFT calculations. In some examples, X-ray crystallography and NMR spectroscopy also represented useful spectroscopic tools to study these complexes in the solid state or in solution. As guest molecules of different nature have been investigated, we have divided the studies of neutral and charged species. Moreover, neutral guests can be also decomposed into two different classes of compounds: the chiral guest species and the achiral ones like xenon. Due to the large number of examples reported with xenon as a guest, a specific section will be dedicated for this species.

### 5.1. Binding of chiral guests with enantiopure cryptophane derivatives

CHFClBr was the first chiral compound to be studied with optically active cryptophane derivatives. These experiments have been carried out in order to estimate the magnitude of the specific optical rotation of the two enantiomers of the CHFClBr derivative, whose $[\alpha]_D$ value has been calculated to be very small. The cavity of the *anti*-**5** is particularly well suited to accommodate the CHFClBr molecule and the openings in this cryptophane permit CHFClBr to access easily its cavity.[1] The use of an optically active *anti*-**5** in presence of *rac*-CHFClBr in $CHCl_3$ led to weak binding constants and to a small enantioselectivity,[88] which is characterized on the $^1$H NMR spectrum by the presence of two couplets of signals with different intensities above room temperature. It was thus observed that the *MM*-(-)-**5** binds more strongly the (-)-CHFClBr enantiomer than its (+)-CHFClBr

congener. These experiments led to an estimated weak difference of the free enthalpy of complexation of $(\Delta\Delta G^0)_{exp}$ = 1.1 kJ mol$^{-1}$. A theoretical approach was used to reproduce these experimental results.[89] Thus, molecular dynamics (MD) first performed on the host-guest system using an explicit solvent model and free energy calculations confirm that the (*R*)-(-)-CHFClBr@*MM*-(-)-**5** diastereoisomer is more stable than the (*S*)-(-)-CHFClBr@*MM*-(-)-**5** complex. The calculated difference of free enthalpy of complexation was found to be in the range $(\Delta\Delta G^0)_{calc}$ = 0 - 2.6 kJ mol$^{-1}$ in a good agreement with the experimental $(\Delta\Delta G^0)_{exp}$ value. The absolute configuration of CHFClBr was later ascertained by using ROA spectroscopy combined with a theoretical approach (MP2/DZP basis set).[90]

An enantio-enriched sulfur-containing cryptophane, *anti*-**59**, with larger cavities have also been studied in presence of chlorofluoiodoromethane (CHFClI) (Figure 27).[56] $^{19}$F NMR spectroscopy has been used to distinguish between these two diastereomeric species, allowing the determination of the binding constants. Thus, small binding constants K = 37 M$^{-1}$ and K = 29 M$^{-1}$ (error estimated to be 15%) were measured for the two (*R*)-(-)-CHFClI@*PP*-(-)-**59** and (*S*)-(+)-CHFClI@*PP*-(-)-**59** diastereomers, respectively. Subsequent experiments with the *PP*-(-)-**59** enantiomer allowed the determination of the enantiomeric excess of the CHFClI derivatives, which has been estimated to be around ee = 23 ± 3 %.

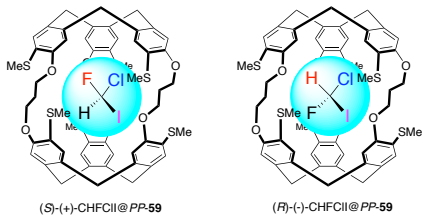


FIGURE 27: Structure des complexes (*S*)-(-)-CHFClI@*PP*-(-)-**59**. and (*R*)-(+)-CHFClI@*PP*-(-)-**59**.

Small chiral oxiranes derivatives such as methyloxirane (called also propylene oxide (PrO), $V_{vdw}$ = 57 Å$^3$), chloromethyloxirane (called also epichlorohydrin, $V_{vdw}$ = 72 Å$^3$), ethyloxirane ($V_{vdw}$ = 74.2 Å$^3$) and bis-oxirane ($V_{vdw}$ = 70.6 Å$^3$) are also well recognized by cryptophane derivatives bearing ethylenedioxy linkers.[91,92,93] For instance, it has been shown that the two enantiomers of methyloxirane fit well the cavity of *anti*-**47** in basic aqueous solution. Thanks to the strong shielding effect of the benzene rings surrounding the guest molecule, the proton signals in the $^1$H NMR spectrum of the encapsulated guest are observed at lower frequencies than those of the free guest in solution. In the case of the PrO@**47** complex they appear at a negative chemical shift values (reference TMS), thus facilitating their identification. Interestingly, the two enantiomers of methyloxirane behave differently in presence of a single enantiomer of *anti*-**47**. For instance, the (*S*)-PrO@*MM*-**47** distereomer shows four distinct $^1$H NMR signals between -0.4 and -2.0 ppm, whereas the (*R*)-PrO@*MM*-**47** diastereomer displays only three $^1$H NMR signals in the same region.[91] In NaOD/$D_2O$ (0.1 M) at 275 K, a small enantioselectivity was observed between the two enantiomers (R) and (*S*)-methyloxirane and the *MM*-**47** enantiomer. Thus, binding constants K = 146 M$^{-1}$ and K = 309 M$^{-1}$ have been measured for the (*R*)-PrO@*MM*-**47** and the (*S*)-PrO@*MM*-**47**, respectively. The use of the *PP*-**47** enantiomer resulted in similar binding constants with an enantioselectivity in favor of the (*R*)-PrO@*PP*-**47** diastereomer. Interestingly, it was noticed that these two diastereomeric complexes give rise to different ECD spectra when recorded in the same experimental conditions. Thus, at 275 K in NaOD/$D_2O$ (0.1 M), the ECD spectra show small but clear differences in the 280 – 320 nm $^1L_b$ spectral region that enables us to distinguish between these two species (Figure 28). In addition, the similarities observed in the ECD spectra between the (*S*)-PrO@*MM*-**47** and the (*rac*)-PrO@*MM*-**47** allows us to ascertain the preference of *MM*-**47** for the (*S*)-PrO enantiomer, in agreement with the NMR data.[91] A change of the structure of the host molecule affects both the enantioselectivity and the recognition process. For instance, lower enantioselectivity was observed with compound **48**, a cryptophane decorated with six carboxylic acid groups, and no changes of the ECD spectra were observed when enantiopure compound **48** was mixed with (*R*)-PrO, (*S*)-PrO or (*rac*)-PrO.[92]

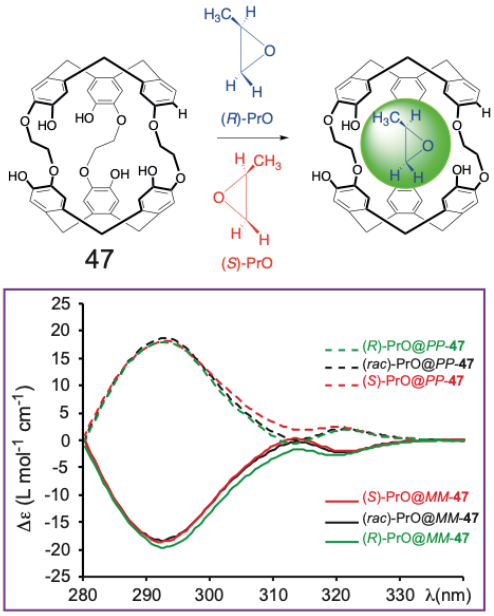


FIGURE 28: Left) Preferential encapsulation of (*R*)-PrO by cryptophane *PP*-**47**. Right) ECD spectra recorded at 275 K of diastereomers (*R*)-PrO@*MM*-**47**, (*S*)-PrO@*MM*-**47** and (*rac*)-PrO@*MM*-**47**, (*R*)-PrO@*PP*-**47**, (*S*)-PrO@*PP*-**47** and (*rac*)-PrO@*PP*-**47**. Only the Cotton bands corresponding to the $^1L_b$ transition are shown. Adapted with permission from ref. 91. (2011) American Chemical Society.

Chloromethyloxirane and ethyloxirane guest molecules showed a similar behavior in presence of an enantiomer of **47**.[93] For instance, clear $^1$H NMR signatures have been observed for each diastereomeric species. Lower enantioselectivity was observed

for these two guests compared to the methyloxirane and a clear correlation was established between the size of the guest molecule and the measured binding constants.[92] On the other hand, dimethyloxirane does not show any affinity for host **47** whereas the two enantiomers of ethyloxirane can access the cavity of this host.[93] As observed, in the case of methyloxirane, different ECD spectra have been obtained in the $^1L_b$ region with the two enantiomers of chloromethyloxirane.

Another original example has been reported with the bioxirane (Bo) derivative.[93] This compound is made of two covalently bonded oxirane cycles. Thus, this molecule contains two stereogenic centers and three stereoisomers are possible for this molecule: (2*R*,2'*R*)-Bo, (2*S*,2'*S*)-Bo and the meso derivative (2*S*,2'*R*)-Bo = (2*R*,2'*S*)-Bo. Thus, in presence of compound **47**, three diastereomeric complexes can be observed with this guest in solution. For instance, at 278 K in NaOD/$D_2O$ (0.1 M), the $^1H$ NMR spectrum of the (*meso*)-Bo in presence of *PP*-**47** resulted in six distinct $^1H$ NMR signals located between 1.0 and -1.4 ppm (Figure 29). In this example, each pair of protons ($H_x$, $H_{x'}$) that composes the bioxirane molecule is enantiotopic. In contrast, only three distinct $^1H$ NMR signals were observed for the two other diastereomeric complexes (2*R*,2'*R*)-Bo@*PP*-**47** and (2*S*,2'*S*)-Bo@*PP*-**47** as a consequence of the homotopic character of each pair of protons ($H_x$, $H_{x'}$). Enantioselectivity was also assessed by $^1H$ NMR spectroscopy and it was observed that the (2*S*,2'*S*)-Bo and the (*meso*)-Bo have better affinity for compound **47**. The ECD spectra of the different diastereomers recorded in the same experimental conditions have also revealed small but clear differences in the $^1L_b$ spectral region, as observed with other oxirane derivatives.

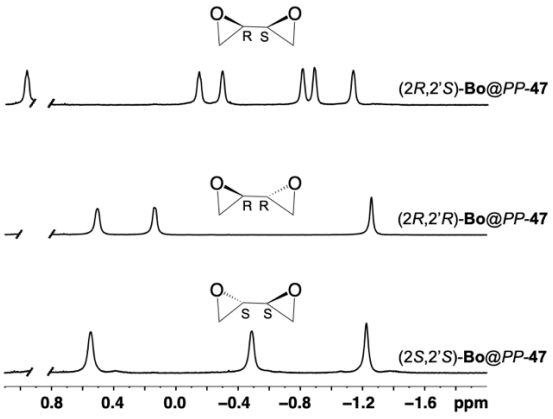


FIGURE 29: $^1H$ NMR (400 MHz) spectrum of (2*R*,2'*S*)-Bo@*PP*-**47**, (2*R*,2'*R*)-Bo@*PP*-**47** and (2S,2'S)-Bo@*PP*-**47.** Only the $^1H$ NMR signals corresponding to the encapsulated guest are shown. Adapted from Ref. [93] with permission from Wiley-VCH Verlag GmbH & Co, Copyright 2018.

### 5.2. Binding of achiral guest molecules with enantiopure cryptophanes

A large spectrum of guest molecules has been studied with optically active cryptophane and their congeners. Unfortunately, very few studies have been reported concerning the effect of these guests on the chiroptical properties of the host molecule. Among these guest molecules, halogenomethane derivatives have been studied under different experimental conditions. Different halogenomethane molecules, especially the chlorinated ones, can easily enter the cavity of cryptophane derivatives. For instance, $CH_2Cl_2$ ($V_{vdw}$ = 57 Å$^3$) and $CHCl_3$ ($V_{vdw}$ = 72 Å$^3$) are currently used as solvents to dissolve cryptophane derivatives. 1,1,2,2-tetrachloroethane ($V_{vdw}$ = 104 Å$^3$) has also been used as solvent but this compound is too large to enter the cavity of small cryptophane derivatives such as *anti*-**1**, *anti*-**9** or even *anti*-**10**. However, Haberhauer and co-workers showed that, this solvent can accommodate the cryptophane-E cavity.[94] As exemplified in part 1, the possibility for a solvent molecule to enter the cavity of cryptophane derivatives has a strong impact on the conformation adopted by the three linkers, which in turn modifies the chiroptical properties of the host molecule. This solvent effect can be easily evidenced on the VCD spectra of different cryptophane molecules. The nature of the solvent molecule also impacts the optical rotation values measured by polarimetry. Thus, a correlation has been clearly observed between the magnitude of SOR values measured and the nature of the solvent molecule present inside the cavity of the host. For instance, the SOR value measured at 589 nm in $CHCl_3$ for the (*PP*)-(+)-**45** derivative is $[\alpha]^{25}_D$ = +255.5 $10^{-1}$ deg cm$^2$ g$^{-1}$ (c = 0.15) and decreases to $[\alpha]^{25}_D$ = + 203.3 $10^{-1}$ deg cm$^2$ g$^{-1}$ (c = 0.15) for $CH_2Cl_2$ that is smaller in volume. A lower value $[\alpha]^{25}_D$ = +147.3 $10^{-1}$ deg cm$^2$ g$^{-1}$ (c = 0.17) has been measured in 1,1,2,2-tetrachloroethane for the guest-free **45**. These results show that it is possible to establish a correlation between the conformation adopted by the linkers and the magnitude of the SOR values. It was noticed that a change of the nature of the solvent also affects slightly the ECD spectrum of cryptophane derivatives, especially for the Cotton bands of the $^1L_b$ transition located at high wavelengths (260-310 nm).[62]

Cryptophane derivatives decorated with acetate moieties exhibit similar behavior. For instance, *anti*-**60** (Figure 30) shows poor solubility in most organic solvents such as $CHCl_3$, $CH_2Cl_2$, DMF or even DMSO. This behavior can be explained by the difficulties for solvents molecules to access the cavity of this host. Low SOR values at 589 nm have been measured in these solvents $[\alpha]^{25}_D$ = -19.8 $10^{-1}$ deg cm$^2$ g$^{-1}$ ($CHCl_3$; c = 0.16) and $[\alpha]^{25}_D$ = -10.2 $10^{-1}$ deg cm$^2$ g$^{-1}$ ($CH_2Cl_2$; c = 0.17) and $[\alpha]^{25}_D$ = -3.9 $10^{-1}$ deg cm$^2$ g$^{-1}$ (DMF; c = 0.18) for the (*PP*)-**60** host derivative.[95] Interestingly, it was noticed that the poor binding properties of this cryptophane forces the molecule to adopt an imploded conformation. Other cryptophane derivatives decorated with different groups show a similar behavior.[68,96,97]

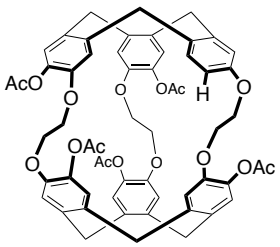


*PP*-**60**

FIGURE 30: Structure of cryptophane (*PP*)-**60**.

Other unusual conformers can be observed with these host molecules, when being unable to accommodate solvent molecules, as for example cryptophane-**56**, which possesses six acetate substituents grafted on the benzene ring and an additional one grafted on a linker.[68] In $CH_2Cl_2$ solution, the solvent can fill easily the cavity of cryptophane-**56** which presents the usual globular shape characteristic of cryptophane derivatives (Figure 31, left). In contrast, in 1,1,2,2-tetrachloroethane, which is too large to fill the cavity, the propylenedioxy linker operates an important conformational rearrangement, allowing the acetate group to point inward the cavity (Figure 31, right). This conformational rearrangement is accompanied with large modifications of the SOR values. Cryptophanes **57** and **58** show a similar behavior. For these compounds, the IR spectroscopy was found to be the best spectroscopic tool to characterize the self-encapsulation process.[68]

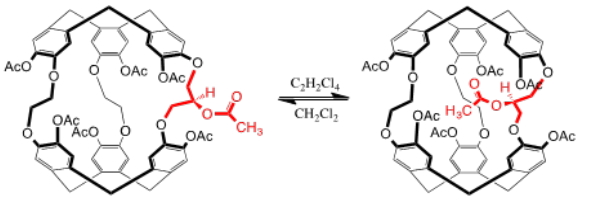


Figure 31: Structure of (*PP*)-**56** and specific optical rotation values reported as a function of the nature of the solvent.

The investigation of cryptophane by polarimetry has revealed that the sign of the SOR values depends on the experimental conditions (solvents, concentration, absence or presence of a guest). Indeed, the change of latter induces conformational variations in cryptophanes' skeleton, which in turn affects the SOR values. For instance, the complexation of $Cs^+$, $Tl^+$ leads to a change of the sign of the SOR values of water-soluble cryptophanes **46** and **47**. The recognition of cationic species by these cryptophanes also results in an important modification of the conformation of the linkers since they are able to establish strong interaction with $Cs^+$ and $Tl^+$.

Generally, the variation of the SOR values (or ORD curves) with the nature of the solvent is accompanied with a notable change of the ECD spectra. Indeed, the spectral dependency of these two techniques are related by the Kramers-Kronig relations and the knowledge of one spectrum theoretically makes it possible to deduce the other.[98] However, several studies reported for cryptophane derivatives have shown that a significant change in ORD curves is not necessarily accompanied by a change in the corresponding ECD spectra, at least for the low-energy Cotton bands (220 - 320 nm). An interesting example has been reported with the *anti*-**53**.[66] Compound **53** has a greater flexibility compared to its congeners due to the absence of extra-substituents attached to its backbone. In this example, the SOR values measured in different solvents show a very peculiar behavior compared to those measured for *anti*-**1**. Indeed, a significant change of the SOR values was observed as a function of the nature of the solvent whereas the ECD spectra remain unchanged at least for the low-energy transitions $^1L_b$ and $^1L_a$. In addition, contrary to results obtained in $CH_2Cl_2$ solution, a change of the sign of the SOR values occurs in the non-resonant region in $CHCl_3$ solution. Different assumptions have been proposed to explain this surprising behavior. For instance, a contribution of the solvent (chiralization of the solvent) to the measured SOR values has been envisaged but this assumption is difficult to verify experimentally. In addition, cryptophane derivatives represent large objects and the use of a theoretical explicit model seems difficult to be applied with these molecules. Nevertheless, a contribution of the solvent in the measured SOR values cannot be totally excluded as it has already been reported with smaller molecules such as methyloxirane.[99,100] On the other hand, a contribution of the high-energy excited states can also be envisaged to explain the differences observed in the SOR values as a function of the solvent. For example, the SRCD spectra recorded in $CHCl_3$ and $CH_2Cl_2$ show clear spectral differences for *PP*-**53** and *MM*-**53** in the high-energy region, which can be due to conformational changes of the ethylenedioxy linkers. A theoretical DFT approach (B3PW91/6-31G** level) allowing to calculate the SOR values for different conformers of **53** has revealed a clear dependence of the SOR values as a function of the conformation adopted by the three linkers.[66] Thus, it was found for this host that a preferential *g*- conformation of the linkers (*g*-, *g*-, *g*+) was preferred in $CH_2Cl_2$ solution. In contrast, a higher proportion of $g_+$ conformation (*g*+, *g*+, *g*-) was observed in $CHCl_3$ solution. The $g_+$ conformer tends to enlarge the cavity of the host compared to the g- conformer, thus facilitating the encapsulation of larger molecules like $CHCl_3$. The assumption that the encapsulation of solvent molecules can modify the SOR values of cryptophane derivatives was confirmed by studying the *anti*-**54** derivative.[65] This compound is unable to accommodate chlorinated solvents such as $CH_2Cl_2$ or $CHCl_3$, and even the $CH_3Cl$ molecule cannot enter its cavity. Thus, the chiroptical properties of this compound were found unchanged and similar SOR values have been measured in these two solvents.

In aqueous solution, cryptophane derivatives bearing hydroxyl functions have revealed a quite different behavior, as their chiroptical properties are strongly dependent on the nature of the halogenated molecule present within the cavity. For instance, the ECD spectrum of *anti*-**46** exhibits large spectral modifications in $NaOH/H_2O$.[73] These spectral changes are more important in the high-energy region of the ECD spectrum and the authors have

established a clear correlation between the molecular volume of the halogenated guest and the intensity of Cotton band measured at 220 nm. Indeed, the larger the size of the halogenated compound the higher the intensity of the Cotton band at 220 nm.[73] The chiroptical changes observed on the ECD spectra are also accompanied by important modifications in the VCD spectra of compound **46** and in the measured SOR values. For instance, for the guest-free *PP*-**46** enantiomer, the SOR value measured at 589 nm in NaOH/$H_2O$ is $[\alpha]^{25}_D$ = - 1.4 $10^{-1}$ deg cm$^2$ g$^{-1}$ (c = 0.21). In presence of $CH_2Cl_2$ and $CHCl_3$, the measured SOR values are $[\alpha]^{25}_D$ = +24.1 $10^{-1}$ deg cm$^2$ g$^{-1}$ (c = 0.16) and $[\alpha]^{25}_D$ = +42.3 $10^{-1}$ deg cm$^2$ g$^{-1}$ (c = 0.19), respectively. It should be noted that the spectral changes observed on the ECD and VCD spectra as well as the changes of the SOR values are dependent on the experimental conditions used. For instance, the replacement of the LiOH/$H_2O$ or the NaOH/$H_2O$ solution by a CsOH/$H_2O$ solution resulted in the absence of spectral modification in the ECD spectra of *PP*-**46**. The strong affinity of the $Cs^+$ cation for the cavity of compound **46** explains this result (see section of cation complexation). Compound **47** showed a similar behavior, as both VCD and ECD spectra were also strongly affected by the nature of the halogenated molecule.[95] The measured SOR values also revealed significant changes in sign and magnitude. For instance, for the guest-free *PP*-**47**, $[\alpha]^{25}_D$ = - 37.1 $10^{-1}$ deg cm$^2$ g$^{-1}$ (c = 0.11) in NaOH/$H_2O$ (0.1M). In presence of $CH_2Cl_2$ and $CHCl_3$, the measured SOR values are $[\alpha]^{25}_D$ = +22.9 $10^{-1}$ deg cm$^2$ g$^{-1}$ (c = 0.11) and $[\alpha]^{25}_D$ = +69.6 $10^{-1}$ deg cm$^2$ g$^{-1}$ (c = 0.11), respectively. Combined all together, these results show a clear correlation between the presence, or the absence, of guest molecules into the cavity of the host and the intensity of the specific optical rotation $[\alpha]^{25}_D$.

### 5.3. Binding of xenon with enantiopure cryptophane derivatives

Xenon-129 appears to be the perfect guest for small cryptophane derivatives as it can establish strong interactions with the cavity of these hosts.[101] The xenon@cryptophane complexes can be easily detected by hyperpolarized $^{129}$Xe NMR spectroscopy, as the xenon-129 isotope possesses a nuclear spin of 1/2. Xenon@cryptophane complexes have been thoroughly studied for two decades especially in the field of supramolecular tracers for MRI applications.[102,103,104,105,106,107] The encapsulated xenon shows high affinity for small cryptophane hosts like *anti*-**54** or *anti*-**1** congeners and large binding constants have been measured with these hosts in organic and in aqueous solution.[97,108] The high affinity of small cryptophane derivatives for xenon lie in their ability to modify their conformation in order to maximize interaction with xenon. Pines and co-workers nicely exemplified this effect by studying the Xe@**1** complex.[109] They were able to establish the conformational changes of the three linkers for the $^{129}$Xe@r*ac*-**1** complex in tetrachloroethane-$d_2$ using $^{129}$Xe-$^1$H SPINOE experiments. Thus, thanks to the determination of the $^1$H-$^{129}$Xe cross-relaxation terms, the inter-nuclear $^1$H-$^{129}$Xe distances have been deduced form these measurements, allowing to establish the preferential *ggg* conformation of the three linkers for the Xe@*rac*-**1** complex. This conformation was consistent with a reduction of the host size when xenon ($V_{vdw}$ = 42 Å$^3$) occupies the cavity.

Interestingly, thanks to the high polarizability of the electronic cloud of xenon, these complexes present a specific $^{129}$Xe NMR signature, far away from the free $^{129}$Xe NMR signals, that can be easily detected. In addition, a tiny change in the surrounding environment of the encapsulated xenon produces a modification of its chemical shift. For instance, this high sensitivity makes it possible to distinguish between cryptophane derivatives that differ only by their number of deuterium atoms or between different diastereomers present in solution.[110] Pines and co-workers have elegantly illustrated the high sensitivity of the xenon atom by synthesizing a biosensor capable of binding to the avidin protein.[111] In this example, the free biosensor present in solution as a mixture of diastereomers, shows several characteristic $^{129}$Xe NMR signals close to each other. The diastereomers result from the use of a cryptophane in its racemic form and the presence of undefined stereogenic centers on the linker bearing the recognition site. The presence of several diastereomers can complicate the interpretation of $^{129}$Xe NMR and the use of a single species seems preferable in some cases. To illustrate this, Berthault and co-workers have prepared and studied separately through $^1$H and $^{129}$Xe NMR spectroscopy two diastereomeric compounds *PM*-**61** or *MP*-**61** in organic solution (Figure 32).[112] These diastereomers resulted from a coupling reaction between the cryptophanol enantiomers and (*S*)-(-)-camphanic acid chloride. Upon complexation with xenon in 1,1,2,2-tetrachloroethane-$d_2$, these two diastereomeric complexes exhibit large chemical shift differences ($\delta$ = 7 ppm) and notable difference in the binding constants was measured. Extensive conformational and dynamic studies have revealed that the more stable diastereomeric complex can more easily deform its structure to accommodate the xenon atom. In contrast, the less stable diastereomeric complex has a stiffer structure that makes xenon complexing less favorable.

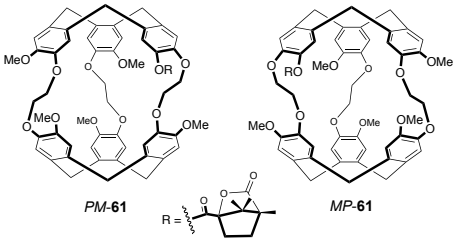


Figure 32: Structure of the two diastereomers *PM*-**61** and *MP*-**61.**

As the use of enantiopure cryptophane enables to interpret more easily the $^{129}$Xe NMR spectra, several cryptophane derivatives have been used in their enantiopure form to design chiral biosensor derivatives. For instance, Berthault and co-workers reported the synthesis of a functionalized biosensor capable to recognize a DNA strand.[17] At a very low concentration in water, a chemical shift is observed in presence of the complementary DNA strand. In contrast, in presence of a non-complementary DNA strand, the $^{129}$Xe NMR signal of the biosensor remains unchanged.

Dmochowski and co-workers reported the synthesis of the two enantiomers of a tris-functionalized cryptophane-A congeners, in which a single propargylic group has been used to introduce a benzenesulfonamide linker whereas water-solubilizing substituents are introduced on the two other functionalities.[113] Upon complexation with the protein carbonic anhydrase II (CAII), each enantiomer binds to CAII and produces diastereomeric complexes, which are characterized by $^{129}$Xe NMR signals shifted by several ppm with respect to the free biosensor dissolved in the bulk. In this example, the authors have identified two specific $^{129}$Xe NMR signals for each enantiomer that suggest a two-sites binding for these biosensors. This finding seems consistent with X-ray crystallographic data suggesting that the benzenesulfonamide moiety can occupy a second site near the surface of the protein.

Rousseau and co-workers reported the synthesis and the $^{129}$Xe NMR study of biosensors used to detect the $Zn^{2+}$ cation at low concentration in water.[114,115] Thus, a single nitrilotriacetic acid (NTA) function was grafted on a carboxylic acid moiety of the water-soluble cryptophane-**48**. Two versions of this biosensor have been prepared: the first version uses compound **48** in its racemic form and the second version uses enantiopure compounds *MM*-**48** and *PP*-**48**. Thus, in the first version, two diastereomeric species co-exist in solution when the NTA moiety is grafted on (*rac*)-**48**, as the NTA group possesses a stereogenic center. In the second version, the biosensor is made of a single enantiomer. In presence of $Zn^{2+}$, the $^{129}$Xe NMR spectrum of the solution containing the two diastereomers reveals two signals of the same intensity suggesting that xenon can distinguish between these two species. This assumption was supported by the use of the enantiopure version (compound **62** on Figure 33) of this biosensor that reveals a single $^{129}$Xe NMR signals in the same conditions. Subsequent $^{129}$Xe NMR experiments have demonstrated that concentration as low as 30 nM of the $Zn^{2+}$ could be easily detected by this approach in few seconds. The same enantiopure biosensor has been exploited to detect in a single $^{129}$Xe NMR experiment several cationic species. In these experiments, each $M^+ \subset {}^{129}$Xe@biosensor complexes (where $M^+$ = $Pb^{2+}$, $Zn^{2+}$, and $Cd^{2+}$) is characterized by a single $^{129}$Xe NMR signal. This multiplexing experiment in which a single biosensor can rapidly detect several analytes in a single experiment illustrates the use of enantiopure cryptophane in the construction of $^{129}$Xe NMR biosensor for MRI application.

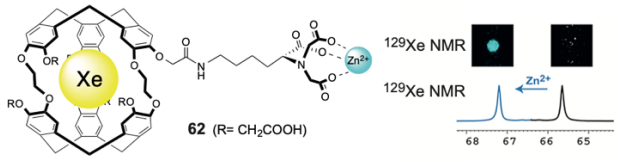


FIGURE 33: (left) Structure of the *MM*-cryptophane-(*L*)-NTA diastereomer **62**. (right-bottom) Chemical shift of encapsulated xenon before and after complexation of $Zn^{2+}$. (right-top) $^{129}$Xe axial gradient-echo fast imaging of an 8 mm tube containing sensor *rac*-**62** at 200 µM before and after addition of $Zn^{2+}$ (100 µM) in the solution. Adapted from Ref. [114] with permission from Wiley-VCH Verlag GmbH & Co, Copyright 2018.

Rousseau and co-workers developed a similar strategy to prepare a doubly responsive probe for the detection of Cys4-tagged proteins.[116] The authors reported the synthesis of the enantiopure compound **63** in which a CRASH probe was grafted on enantiopure compound **48** (Figure 34). The CRASH probe has been extensively used by biochemists to detect specifically the tetra-cystein Cys-Cys-X-X-Cys-Cys sequence in proteins, where X is an amino acid except cysteine. Upon complexation with the short peptide Ace-WEAAAREACCRECCARA-$CONH_2$ capable of forming a $\alpha$-helix, a strong increase in the fluorescence of the CRASH probe is observed and the encapsulated $^{129}$Xe signal is subjected to a displacement of several ppm with respect to the dissolved biosensor in solution (Figure 33). The use of two independent detection modes is useful to ensure that the effective molecular recognition process has taken place. This approach is particularly interesting for in cellulo experiments where fluorescence can be used to ascertain cell-uptake. Using a similar strategy, Erard and co-workers reported the synthesis of several bimodal CRASH probes where the position of the linkers on the benzene ring of the CRASH probe varies.[117] Using hyperpolarized $^{129}$Xe and fluorescence spectroscopy the authors showed that the ability of the bio-probe to detect a Cys4-tagged protein depends both on the cryptophane stereomer chosen for the experiment and the nature of the Cys4-tag.

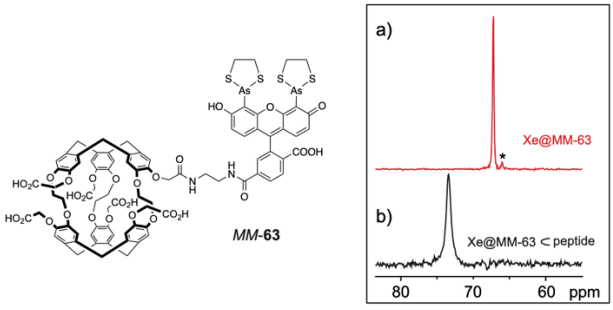


FIGURE 34: Structure of the CRASH probe. High field part of the one-scan $^{129}$Xe NMR spectrum of a 25 µM solution of *MM*-**63** in phosphate buffer. a) *MM*-**63** alone; b) in the presence of 10 equivalents of the peptide. The star denotes residual *MM*-**48**. Reproduced from Ref. 116 with permission from The Royal Society of Chemistry.

Brotin and Buffeteau investigated the two enantiomers of compound **54** and its complex with xenon by VOA spectroscopies.[65] The VCD spectrum of the Xe@*MM*-**54** complex was found identical to that of compound *MM*-**54** recorded in $CD_2Cl_2$. Interestingly, the ROA spectra recorded between 1800 and 100 $cm^{-1}$ are identical for compound *MM*-**54** and the Xe@*MM*-**54** complex, except in the 200-100 $cm^{-1}$ spectral region that shows the disappearance of a band at 150 $cm^{-1}$ for the Xe@*MM*-**54** complex (Figure 35). DFT calculation revealed that this band could be associated to the breathing mode of the cage.

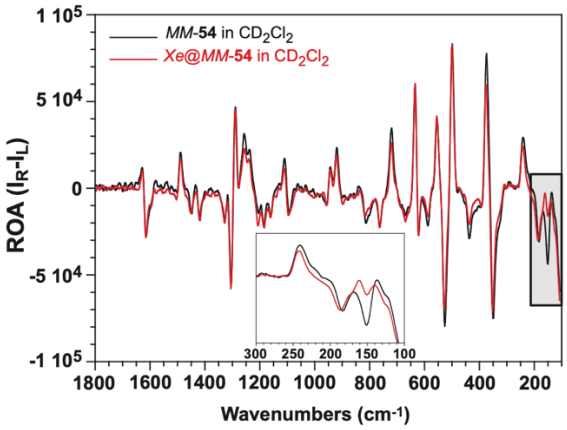


FIGURE 35: Comparison of experimental ROA spectra of *MM*-**54** in $CD_2Cl_2$ solution in presence (red spectrum) or not (black spectrum) of xenon. Reproduced from Ref. 65 with permission from The Royal Society of Chemistry.

Nitschke and co-workers reported the synthesis of molecular superstructure in which an enantiopure *anti*-**54** is encapsulated into a larger inorganic host structure.[118] In turn, the authors demonstrated that the encapsulated cryptophane host could accommodate a xenon atom. As the inorganic superstructure itself is chiral, the association with an enantiopure *anti*-**54** opens the possibility to form several diastereomeric species. Interestingly, the authors have observed a stereochemical information transfer from the inner cage to the self-assembled capsule. This observation was ascertained by ECD spectroscopy and X-ray crystallography. Thus, the Xe@*PP*-**54** derivative, in presence of a racemic mixture of inorganic cages $\Delta$ and $\Lambda$, leads almost exclusively to the formation of the [Xe@*PP*-**54**]$\subset\Delta_4$-$Fe^{II}_4L_4$ supramolecular complex. In turn, the [Xe@*MM*-**54**]$\subset\Lambda_4$-$Fe^{II}_4L_4$ complex was preferentially formed in presence of the Xe@*MM*-**54** complex and a racemic mixture of inorganic cages $\Delta$ and $\Lambda$. A high binding constant $K = 9.5\ 10^6\ M^{-1}$ has been measured between the *PP*-**54** enantiomer and the cage $\Delta_4$-$Fe^{II}_4L_4$ whereas the same enantiomer shows a lower association constant $K = 1.8\ 10^4\ M^{-1}$ with the $\Lambda_4$-$Fe^{II}_4L_4$ superstructure. Thanks to the use of hyperpolarized $^{129}Xe$, a characteristic signal for these two complexes can be easily detected at 47 ppm. Interestingly, it was shown that the encapsulated xenon can sense the chirality of the outermost inorganic cage and the authors reported that the encapsulated xenon present in the two diastereomers [Xe@*PP*-**54**]$\subset\Delta_4$-$Fe^{II}_4L_4$ and [Xe@*PP*-**54**]$\subset\Lambda_4$-$Fe^{II}_4L_4$ structures shows different $^{129}Xe$ NMR signatures. Particularly, one $^{129}Xe$ NMR signal appears to be deshielded with respect to the Xe@*anti*-**54** complex whereas the other $^{129}Xe$ NMR signal is shielded by the same magnitude with respect to this complex.

### 5.4. Binding of cationic species

Water-soluble cryptophane derivatives also show high affinity for cationic species in aqueous solution such as the alkali cations $Rb^+$ and $Cs^+$ as well as the highly toxic $Tl^+$ (thallium-(I)) cation. So far, efficient complexation has been limited to cryptophane derivatives bearing several hydroxyl functions whereas water-soluble derivatives bearing other functionalities do not show any affinity for these cationic species.[119,120,121] Basic aqueous solutions have been found to be mandatory to ensure good solubility of these cryptophane hosts. Thus, compounds **46**-**47** show very high affinity for $Cs^+$ and $Tl^+$ under these conditions. Several techniques, such as $^{133}Cs$ and $^{205}Tl$ NMR spectroscopy, have been used to characterize $Cs^+$@**46**-**47** and $Tl^+$@**46**-**47** complexes, since these complexes display characteristic NMR signatures at low frequencies with respect to the metal ion dissolved in the bulk. With these two highly polarizable cations the difference of chemical shift is huge and it exceeds several hundreds of ppm. On the other hand, isothermal calorimetric titration (ITC) allows the determination of the thermodynamic parameters of complexation under various conditions and large association constants have been measured with this technique in $LiOH/H_2O$ and $NaOH/H_2O$ (0.1 M). For instance, binding constant as large as $K = 5.3\ 10^8\ M^{-1}$ have been measured in $NaOH/H_2O$ for the $Cs^+$@**47** complex.[120] Interestingly, ECD and VCD spectroscopy also afford important information about these two complexes. For instance, Brotin and co-workers reported the evolution of the ECD spectra of a series of $M^+$@cryptophane complexes ($M^+ = Rb^+$, $Cs^+$, $Tl^+$) in $NaOH/H_2O$, $LiOH/H_2O$ and $KOH/H_2O$ solutions.[120] In particular, significant changes are observed in the ECD spectrum of *anti*-**47** upon addition of small amounts of $Cs^+$ but this evolution stops when more than one equivalent of $Cs^+$ is added to the solution (Figure 36). In addition, it was observed that the absence or the presence of guest molecule initially present ($CHCl_3$) within the host-cavity plays a key role in the evolution of the ECD spectrum.[119] The most significant spectroscopic changes are observed in the high-energy region of the ECD spectrum where a strong decrease in the intensity of the Cotton band located at 220 nm is observed upon addition of $Cs^+$ (Figure 36b). The lack of $CHCl_3$ within the host-cavity gives rise to less pronounced spectral changes (Figure 36a). Thus, a clear correlation between the cage occupancy and the conformation of the linkers can be established. For instance, the presence of a $CHCl_3$ molecule enlarges the host-cavity and forces the linkers to adopt a preferentially *ttt* conformation. A change of guest, whose van der Waals volume is significantly smaller, results in a preferentially *ggg* conformation of the linkers. Several independent observations confirm this result. For example, replacing $Cs^+$ with $Rb^+$ results in similar ECD spectra and suggests that the shape of the ECD spectrum is not directly related to the nature of the alkali cation. In addition, the ECD spectrum of $Cs^+$@**47** complex remains almost unchanged in $KOH/H_2O$ when $Cs^+$ is added to the solution.[120] In this example, the $K^+$ cation is also recognized by host **47** with a significantly lower association constant $K \sim 1000\ M^{-1}$ than the $Cs^+$ cation. Consequently, the host molecule has already adopted a preferentially *ggg* conformation prior to $Cs^+$ complexation. Hence, the replacement of the $K^+$ cation by another alkali cation such as $Cs^+$ results in moderate changes in the conformation of the linkers, as a result similar ECD spectra are measured. Related observations have been made with the *anti*-**46** and even higher association constants have been measured for the $Cs^+$@**46** complex. Indeed, it has been clearly established that the higher the number of phenol group grafted on the cryptophane skeleton the stronger the host-guest binding constant.

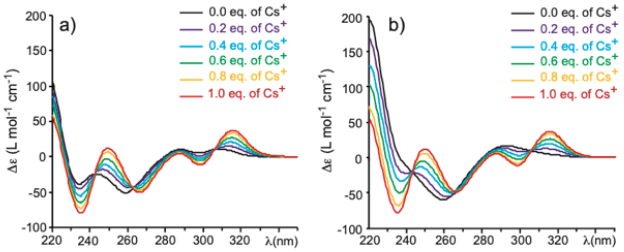


FIGURE 36: ECD spectra recorded at 293 K of *PP*-**47**: a) in 0.1 M $LiOH/H_2O$ solution in the presence of different amounts of a $CsOH/H_2O$ solution; b) in a saturated solution of $CHCl_3$ in $LiOH/H_2O$ in presence of different amounts of a $CsOH/H_2O$ solution. ECD spectra for higher concentration in $Cs^+$ are identical to that recorded for 1.0 eq. of $Cs^+$. Adapted with permission from ref. 119. (2012) American Chemical Society.

Similarly, Brotin and co-workers reported important spectral modifications in the VCD spectra of *PP*-**47**, upon addition of $Cs^+$.[120] Thus, a comparison between the guest-free *PP*-**47**, the $Cs^+$@*PP*-**47** and the $CHCl_3$@*PP*-**47** complexes reveal clear differences that can be attributed to conformational changes upon complexation. For instance, the replacement of $CHCl_3$ by $Cs^+$ leads to a significant decrease of the VCD band located at 1490 $cm^{-1}$ (Figure 37). The intensities of other VCD bands are also affected by the encapsulation process, in particular the intensity of the band located at 1600 $cm^{-1}$ increases as the van der Waals volume of the guest decreases. Brotin and Dognon reported similar results with a water-soluble cryptophane decorated with six phenol groups and an alcohol function positioned on the propylenedioxyl linker.[67]

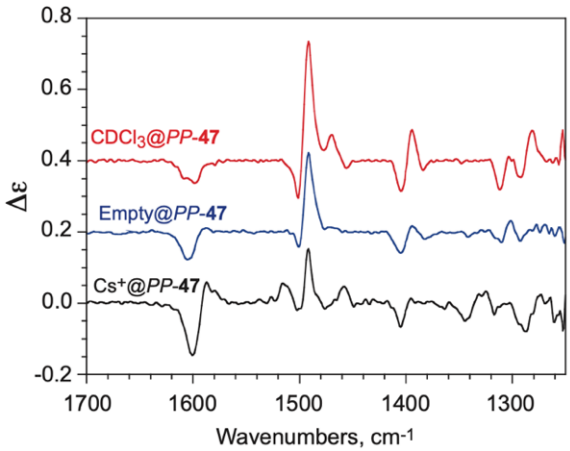


FIGURE 37: VCD spectra recorded at 293 K of empty *PP*-**47** (blue spectrum) as well as $CDCl_3$@*PP*-**47** (red spectrum) and $Cs^+$@*PP*-**47** (black spectrum) complexes in $NaOD/D_2O$ solution (0.21 M). The concentration of host **47** was 0.030 M. Adapted with permission from ref. 119. (2012) American Chemical Society.

Thallium (I) is even more recognized by these cages and its association constants are one order of magnitude larger than that detected for $Cs^+$. The replacement of $Cs^+$ by $Tl^+$ gives rise to similar spectral changes in the high-energy region of the ECD spectrum but the Cotton bands corresponding to the $^1L_b$ transition clearly show a different shape that can be easily recognized. This finding, which is generalized for all the cryptophane studied, suggests a different type of interaction between these molecular hosts and $Tl^+$. An energy decomposition analysis performed on one cryptophane permitted to evaluate the different types of interaction that take place between the host and the metal cation. In the case of $Tl^+$, it was clearly established that π-cation interactions govern the complexation phenomenon between cryptophane and $Tl^+$.[67] This type of interaction is not present with the alkali cations like $Cs^+$ and $Rb^+$.

As it was shown for xenon, Nitschke and co-workers reported the efficient binding of $Cs^+$ by the encaged enantiopure *anti*-**54** (Figure 38).[118] Complexation of $Cs^+$ was clearly established by $^{133}Cs$ NMR spectroscopy and different $^{133}Cs$ chemical shift have been measured for the two diastereomers $[Cs^+$@*PP*-**54**$]\subset\Delta_4$-$Fe^{II}_4L_4$ (δ = 311 ppm) and $[Cs^+$@*PP*-**54**$]\subset\Lambda_4$-$Fe^{II}_4L_4$ (δ = 256 ppm). These examples represent the unusual encapsulation of charged guests within a superstructure of the same charge.

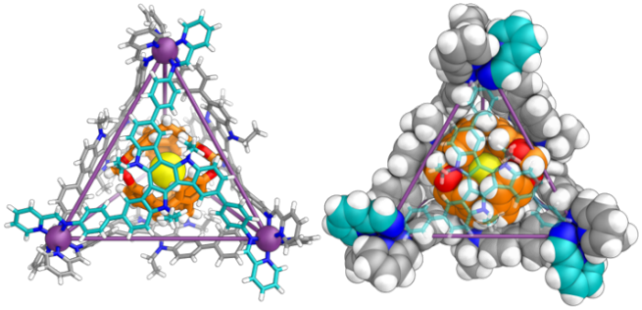

FIGURE 38: Crystal structure of $[Cs^+\subset$*PP*-**54**$]\subset\Delta_4$-$Fe^{II}_4L_4$ illustrating the $[Cs^+\subset$*PP*-**54**$]\subset\Delta_4$-$Fe^{II}_4L_4$ enantiomer. The bound $Cs^+$, *PP*-**54** and the front triazatruxene face are colored yellow, orange and cyan, respectively. Disorder, unbound counterions, and solvent of crystallization are omitted for clarity and only one of the two crystallographically independent complexes is shown. Adapted with permission from ref. 117. (2019) American Chemical Society.

## 6. Conclusion

This review focuses on the synthesis of enantiopure cryptophane derivatives and the study of their chiroptical properties by different chiroptical techniques. Even though numerous interesting results have been obtained in this field by our group and others, the study of the chiroptical properties of cryptophane is still in its infancy. The difficulty of obtaining these molecules in their enantiopure form has been for a long time the main obstacle to the study of their chiroptical properties. However, nowadays, separation methods such as the chiral HPLC

technique allow to rapidly obtain enantiopure material, allowing a thorough study of their chiroptical properties. Consequently, the study of enantiopure cryptophane should be facilitated in the future and should lead to a rapid development of this field.

The synthesis of novel cryptophane structures is another difficulty that chemists have to face with these polyaromatic systems.[122] The introduction of new substituents, in particular electron-withdrawing substituents, constitute a real challenge and should lead to new hosts with original chiroptical properties, different from those reported previously with electron-donating substituents. In addition, the study of chiroptical properties of water-soluble cryptophane bearing pH-sensitive substituents should be encouraged because these systems have revealed great sensitivity upon guest encapsulation. It should be noticed that most of the studies reported in the literature have mainly involved *anti*-cryptophane derivatives. The study of *syn*-diastereomers should also be considered in the future, since their chiroptical properties are expected to be significantly different.

The ability of cryptophanes to isolate a guest molecule in a chiral environment represents one of the most interesting properties of these systems. Thus, chiroptical techniques combined with quantum calculation represent ideal tools to investigate in great details the behavior of guest molecules trapped inside a chiral environment. For instance, the detection of induced chirality effects of chiral hosts on achiral guests has not yet clearly established experimentally and would constitute a real challenge.

Finally, the discrimination of small chiral guests by cryptophane enantiomers makes it possible to fabricate stationary chiral phases based on enantiopure cryptophanes grafted onto solid phases. The preparation of such materials should be now facilitated thanks to the possibility to access enantiopure cryptophanes in reasonable quantities. Such new materials would be valuable to separate small chiral compounds such as chiral oxiranes, azirines, etc… .

**Acknowledgements**

The authors are indebted to the CNRS (Chemistry Department) and to Région Aquitaine for financial support. The GDR 3712 Chirafun is acknowledged for allowing a collaborative network between the partners of this project.

REFERENCES AND NOTES

**1.** Canceill J, Lacombe L, Collet A. Analytical optical resolution of bromochlorofluoromethane by enantioselective inclusion into a tailor-Made "Cryptophane" and determination of its maximum rotation. J. Am. Chem. Soc. **1985**, 107:6993–6996.
**2.** Gabard J, Collet A. Synthesis of a ($D_3$)-bis(cyclotriveratrylenyl) macrocage by stereospecific replication of a ($C_3$)-subunit. Chem. Commun. **1981**, 21:1137–1139.
**3.** Collet A. Cyclotriveratrylenes and cryptophanes. Tetrahedron **1987**, 43:5725-5759.
**4.** a) Brotin T, Dutasta JP, Cryptophanes and their complexes present and future. Chem. Rev. **2009**, 109:88-130.
**5.** El-Ayle G, Holman KT. Cryptophanes, comprehensive supramolecular chemistry II. Elsevier **2017**, 6:199-249.
**6.** Brotin T, Guy L, Martinez A, Dutasta JP, Schurig V. Enantiopure supramolecular cages: synthesis and chiral recognition properties, differentiation of enantiomers II. Springer International Publishing **2013**, 177-230.
**7.** Böhmer V, Kraft D, Tabatabai M. Inherently chiral calixarenes. J. Inclusion Phenom. Mol. Recognit. Chem. **1994**, 19:17-39.
**8.** Brotin T, Jeanneau E, Berthault P, Léonce E, Pitrat D, Mulatier JC. Synthesis of cryptophane-B: crystal structure and study of its complex with xenon. J. Org. Chem. **2018**, 83(23):14465–14471.
**9.** Brotin T, Cavagnat D, Jeanneau E, Buffeteau T. Synthesis of highly substituted cryptophane derivatives. J. Org. Chem. **2013**, 78(12): 6143-6153.
**10.** (a) Taratula O, Hill PA, Bai Y, Khan NS, Dmochowski IJ. Shorter synthesis of trifunctionalized cryptophane-A derivatives. Org. Lett. **2011**, 13(6):1414-1417.
**11.** Delacour L, Kotera N, Traoré T, Garcia-Argote S, Puente C, Leteurtre F, Gravel G, Léonce E, Boulard Y, Berthault P, Rousseau B. "Clickable" hydrosoluble PEGylated cryptophane as a universal platform for $^{129}$Xe magnetic resonance imaging biosensors. Chem. Eur. J. **2013**, 19(19):6089-6093.
**12.** Wei Q, Seward GK, Hill PA, Patton B, Dimitrov IE, Kuzma NN, Dmochowski IJ. Designing $^{129}$Xe NMR biosensors for matrix metalloproteinase detection. J. Am. Chem. Soc. **2006**, 128(40):13274–13283.
**13.** Hill PA, Wei Q, Troxler T, Dmochowski IJ. Substituent effects on Xenon binding affinity and solution behavior of water-soluble cryptophanes. J. Am. Chem. Soc. **2009**, 131(8):3069-3077.
**14.** Joseph A. I, El-Ayle G, Boutin C, Léonce E, Berthault P, Holman T. Rim-functionalized cryptophane-111 derivatives via heterocapping, and their xenon complexes. Chem. Commun. **2014**, 50(100):15905–15908.
**15.** See for instance (a) Darzac M., Brotin T, Bouchu D, Dutasta JP. Cryptophanols, new versatile compounds for the synthesis of functionalized cryptophanes and polycryptophanes. Chem. Commun. **2002**, 48-49.
**16.** Spence MM, Rubin SM, Dimitrov IE, Ruiz EJ, Wemmer DE, Pines A. Yao SQ, Tian, F, Schultz PG. Functionalized xenon as a biosensor. Proc. Natl. Acad. Sci. **2001**, 98(19):10654–10657.
**17.** Roy V, Brotin T, Dutasta JP, Charles MH, Delair T, Mallet F, Huber G, Desvaux H, Boulard Y, Berthault P. A cryptophane biosensor for the detection of specific nucleotide targets through xenon NMR Spectroscopy. Chem. Phys. Chem. **2007**, 8(14):2082–2085.
**18.** Brotin T, Dutasta JP. Xe@Cryptophane complexes with $C_2$ symmetry: synthesis and investigations by $^{129}$Xe NMR of the consequences of the size of the host cavity for xenon. Eur. J. Org. Chem. **2003**, 6:973–984.
**19.** Tambute A, Canceill J, Collet A. Optical resolution of $C_3$ cyclotriveratrylenes and $D_3$ cryptophanes by liquid chromatography on chiral stationary phase chiralpack OT-(+). Bull. Chem. Soc. Jpn. **1989**, 62:1390-1392.
**20.** Canceill. J, Césario, M, Collet A, Guilhem J, Riche C, Pascard C. Selective Recognition of Neutral Molecules: 1H N.M.R. Study of the Complexation of $CH_2Cl_2$ and $CH_2Br_2$ by Cryptophane-D in Solution and Crystal Structure of its $CH_2Cl_2$ Cavitate. J. Chem. Soc., Chem. Commun. **1986**: 339-341.
**21.** Brotin T, Vanthuyne N, Cavagnat D, Ducasse L, Buffeteau T. Chiroptical properties of nona- and dodecamethoxy cryptophanes. J. Org. Chem. **2014**, 79(13):6028–6036.
**22.** Collet A., Gabard G., Jacques J., Césario M., Guilhem J., Pascard C. Synthesis and Absolute Configuration of Chiral ($C_3$) Cyclotriveratrylene Derivatives. Crystal Structure of (*M*)-(−)-2,7,12-Triethoxy-3,8,13-tris-[(R)-1-methoxycarbonylethoxy]-10,15-dihydro-5H-tribenzo[a,d,g]-cyclononene. J. Chem. Soc. Perkin. Trans. 1, **1981**, 1630-1638.
**23.** IUPAC 1968 Tentative Rules, Section E, Fundamental Stereochemistry in J. Org. Chem. **1970**, 35, 2849-2867.
**24.** Lüttringhaus A, Peters KC. Conformational enantiomerism of a derivative of cyclotriveratrylene. Angew. Chem. Int. Ed. **1966**, 5(6):593-594.
**25.** Collet A, Gabard J. Optically active ($C_3$)-cyclotriveratrylene-$d_9$. Energy barrier for the "crown to crown" conformational interconversion of its nine-membered-ring system. J. Org. Chem. **1980**, 45:5400-5401.

**26.** Lutz MR, French DC, Rehage P, Becker DP. Isolation of the saddle and crown conformers of cyclotriveratrylene (CTV) oxime. Tetrahedron Lett. **2007**, 48:6368-6371.
**27.** Collet A. Chromophores chiraux possédant la symmétrie $C_3$. synthèse de dérives optiquement actifs du cyclotriveratrylene. Tetrahedron Lett. **1978**, 15(15):1265–1268.
**28.** IUPAC name: (±)-2,7,12-Trihydroxy-10,15-dihydro-5H-tribenzo[a,d,g] cyclononene.
**29.** Costante J, Garcia C, Collet A. Key intermediates in cyclotriveratrylene chemistry: A new route to the enantiomers of $C_3$-cyclotriphenolene and cryptophane-C. Chirality **1997**, 9:446–453.
**30.** Canceill J, Collet A, Gabard J, Gottarelli G, Spadat GP. Exciton approach to the optical activity of $C_3$-cyclotriveratrylene derivatives. J. Am. Chem. Soc. **1985**, 107:1299-1308.
**31.** Garcia C, Andraud C, Collet A. New key compounds in cyclotriveratrylene chemistry. synthesis, optical resolution, absolute configuration and circular dichroism of $C_3$-cyclotriveratrylenes with sulfur substituents. Supramolecular Chemistry **1992**, 1:31-45.
**32.** Canceill J, Collet A, Gottarelli G. Optical activity due to isotopic substitution. synthesis, stereochemistry, and circular dichroism of (+) and (-)-[ 2,7,1 2-2H,]cyclotribenzylene. J. Am. Chem. Soc. **1984**, 106:5997-6003.
**33.** Rump ET, Rijkers DT, Hilbers HW, de Groot PG, Liskamp RM. Cyclotriveratrylene (CTV) as a new chiral triacid scaffold capable of inducing triple helix formation of collagen peptides containing either a native sequence or pro-hyp-gly repeats. Chem. Eur. J. **2002**, 8(20):4613-4621.
**34.** Yu JT, Huang ZT, Zheng QY, Synthesis, structure, fullerene-binding and resolution of $C_3$-symmetric cavitands with rigid and deep cavities. Org. Biomolec. Chem. **2012**, 10(7):1359-1364.
**35.** Luz Z, Poupko R, Wachtel EJ, Zheng H, Friedman N, Cao X, Freedman TB, Nafie LA, Zimmermann H. Structural and optical isomers of nonamethoxy cyclotriveratrylene: separation and physical characterization. J. Phys. Chem. A **2007**, 111(42):10507-10516.
**36.** Götz S, Schneider A, Lützen A. Efficient resolution of racemic crown-shaped cyclotriveratrylene derivatives and isolation and characterization of the intermediate saddle lisomer. Beilstein J. Org. Chem. **2019**, 15:1339–1346.
**37.** Lefevre S, Zhang D, Godart E, Jean M, Vanthuyne N, Mulatier JC, Dutasta JP, Guy L, Martinez A. Large-scale synthesis of eenantiopure molecular cages: Chiroptical and recognition properties. Chem. Eur. J. **2016**, 22(6):2068-2074.
**38.** Zhang D, Martinez A, Dutasta JP. Emergence of hemicryptophanes: from synthesis to applications for recognition, molecular machines, and supramolecular catalysis. Chem. Rev. **2017**, 117(6):4900-4942.
**39.** Colomban C, Châtelet B, Martinez A. Different strategies for obtaining enantiopure hemicryptophanes. Synthesis **2019**, 51(10): 2081-2099.
**40.** Kraszewska A, Rivera-Fuentes P, Rapenne G, Crassous J, Petrovic AG, Alonso-Gómez JL, Huerta E, Diederich F, Thilgen C. Regioselectivity in tether-directed remote functionalization–The addition of a cyclotriveratrylene-based trimalonate to $C_{60}$ revisited. Eur. J. Org. Chem. **2010**, 2010(23):4402-4411.
**41.** Long A, Colomban C, Jean M, Albalat M, Vanthuyne N, Giorgi M, Di Bari L, Górecki M, Dutasta JP, Martinez A. Enantiopure $C_1$-cyclotriveratrylene with a reversed spatial arrangement of the substituents. Org. Lett. **2018**, 21(1):160-165.
**42.** Xu D, Warmuth R. Edge-directed dynamic covalent synthesis of a chiral nanocube. J. Am. Chem. Soc. **2008**, 130(24):7520–7521.
**43.** Kuck D. Three-dimensional hydrocarbon cores based on multiply fused cyclopentane and indane units: centropolyindanes. Chem. Rev. **2006**, 106:4885.
**44.** Kuck D. Functionalized aromatics aligned with the three cartesian axes: extension of centropolyindane chemistry. Pure Appl. Chem. **2006**, 78:749.
**45.** Strübe J, Neumann B, Stammler HG, Kuck D. Solid-state enantiopure organic nanocubes formed by self-organization of a $C_3$-symmetrical tribenzotriquinacene. Chem. Eur. J. **2009**, 15(10):2256-2260.
**46.** Markopoulos G, Henneicke L, Shen J, Okamoto Y, Jones PG, Hopf H. Tribenzotriquinacene: A versatile synthesis and $C_3$-chiral platforms. Angew. Chem. Int. Ed. **2012**, 51(51):12884-12887.
**47.** Xu WR, Chow HF, Cao XP, Kuck D. Regiocontrolled synthesis and optical resolution of mono-, di-, and trisubstituted tribenzotriquinacene derivatives: key building blocks for further assembly into molecular squares and cubes. J. Org. Chem. **2014**, 79(19):9335-9346.
**48.** Xu WR, Chow HF, Cao XP, Kuck D. Correction to regiocontrolled synthesis and optical resolution of mono-, di-, and trisubstituted tribenzotriquinacene derivatives: key building blocks for further assembly into molecular squares and cubes. J. Org. Chem. **2015**, 80(8):4221-4222.
**49.** Xu WR, Wang XR, Chow HF, Kuck D. Synthesis and characterization of enantiopure tribenzotriquinacene dimers bearing a platinum-diacetylene unit. Synthesis **2019**, 51(10):2116-2121.
**50.** Beaudoin D, Rominger F, Mastalerz M. Synthesis and chiral resolution of $C_3$-symmetric tribenzotriquinacenes. Eur. J. Org. Chem. **2016**, 2016(26):4470-4472.
**51.** Wagner P, Rominger F, Mastalerz M. Switching the statistical $C_3/C_1$ ratio in the threefold aromatic substitution of tribenzotriquinacenes towards the $C_3$ isomer. Angew. Chem. Int. Ed. **2018**, 57(35):11321-11324.
**52.** Wagner P, Rominger F, Oeser T, Mastalerz M. Solvent-controlled racemic resolution of $C_3$-symmetric trihydroxytribenzotriquinacenes. J. Org. Chem. **2020**, 85(5):3981-3989.
**53.** Wang T, Zhang YF, Hou QQ, Xu WR, Cao XP, Chow HF, Kuck D. $C_3$-symmetrical tribenzotriquinacene derivatives: optical resolution through cryptophane synthesis and supramolecular self-assembly into nanotubes. J. Org. Chem. **2013**, 78(3):1062-1069.
**54.** Canceill J, Collet A, Gottarelli G, Palmieri P. Synthesis and exciton optical activity of $D_3$-cryptophanes. J. Am. Chem. Soc. **1987**, 109(21):6454-6464.
**55.** Gabard J, Canceill J, Collet A. New $D_3$ and $C_{3h}$ cryptophanes with ethelynic bridges structural assignments, absolute configurations and circular dichroism of $D_3$ isomers. Tetrahedron **1987**, 43(20):4531–4538.
**56.** Soulard P, Asselin P, Cuisset A, Moreno A, Huet J. R, Petitprez TR, Petitprez D, Demaison J, Freedman TB, Cao X, Nafie LA, Crassous J. Chlorofluoroiodomethane as a potential candidate for parity violation measurements. Phys. Chem. Chem. Phys. **2006**, 8(1):79–92.
**57.** Zarra S, Wood DM, Roberts DA, Nitschke JR. Molecular containers in complex chemical systems. Chem. Soc. Rev. **2015**, 44(2):419-432.
**58.** Hardie MJ. Self-assembled cages and capsules using cyclotriveratrylene-type scaffolds. Chem. Lett. **2016**, 45(12):1336-1346.
**59.** Zhong Z, Ikeda A, Shinkai S, Sakamoto S, Yamaguchi K. Creation of novel chiral cryptophanes by a self-assembling method utilizing a pyridyl− Pd (II) interaction. Org. Lett. **2001**, 3(7): 1085-1087.
**60.** Schaly A, Meyer M, Chambron JC, Jean M, Vanthuyne N, Aubert E, Espinosa E, Zorn N, Leize-Wagner E. The chemo- and stereoselective formation of pallado-and platinocryptophanes. Eur. J. Inorg. Chem. **2019**, 2019(22):2691-2706.
**61.** Brotin T, Barbe R, Darzac M, Dutasta JP. Novel synthetic approach for optical resolution of cryptophanol-A: A direct access to chiral cryptophanes and their chiroptical properties. Chem. Eur. J. **2003**, 9(23):5784–5792.
**62.** Cavagnat D, Buffeteau T, Brotin T. Synthesis and chiroptical properties of cryptophanes having $C_1$-symmetry. J. Org. Chem. **2008**, 73(1):66–75.
**63.** Taratula O, Kim MP, Bai Y, Philbin JP, Riggle A, Haase DN, Dmochowski IJ. Synthesis of enantiopure, trisubstituted cryptophane - A derivatives. Org. Lett. **2012**, 14(14):3580–3583.
**64.** Brotin T, Daugey N, Vanthuyne N, Jeanneau E, Ducasse L, Buffeteau T. Chiroptical properties of cryptophane-223 and -233 investigated by ECD, VCD, and ROA spectroscopy. J. Phys. Chem. B **2015**, 119(27):8631–8639.
**65.** Buffeteau T, Pitrat D, Daugey N, Calin N, Jean M, Vanthuyne N, Ducasse L, Wien F, Brotin T. Chiroptical properties of cryptophane-111. Phys. Chem. Chem. Phys. **2017**, 19(28):18303–18310.
**66.** Pitrat D, Daugey N, Jean M, Vanthuyne N, Wien F, Ducasse L, Calin N, Buffeteau T, Brotin T. Unusual chiroptical properties of the cryptophane-222 skeleton. J. Phys. Chem. B **2016**, 120(49):12650–12659.
**67.** Chapellet LL, Dognon JP, Jean M, Vanthuyne N, Berthault P, Buffeteau T, Brotin T. Experimental and theoretical study of the complexation of cesium and thallium cations by a water-soluble cryptophane. ChemistrySelect **2017**, 2(19):5292–5300.
**68.** Baydoun O, Buffeteau T, Daugey N, Jean M, Vanthuyne N, Chapellet LL, De Rycke N, Brotin T. Chiroptical study of cryptophanes subjected to self-encapsulation. Chirality **2019**, 31(7):481-491.
**69.** The sign (+) and (-) used in the absolute configurations reported in section 4 refers to the SOR measured at 589 nm by polarimetry.

**70.** Platt JR. Molecular orbitals prediction of organic spectra. J. Chem. Phys. **1950**, 18:1168-1173.
**71.** a) Harada N, Nakanishi K. Circular dichroism spectroscopy: exciton coupling in organic stereochemistry. University Science Books, Mill Valley, CA, **1983**.
**72.** Harada N, Nakanishi K. Determining the chiralities of optically active glycols. J. Am. Chem. Soc. **1969**, 91(14):3989-3991.
**73.** Bouchet A, Brotin T, Cavagnat D, Buffeteau T. Induced chiroptical changes of a water-soluble cryptophane by encapsulation of guest molecules and counterion effects. Chem. Eur. J. **2010**, 16:4507-4518.
**74.** Brotin T, Cavagnat D, Dutasta JP, Buffeteau T. Vibrational circular dichroism study of optically pure cryptophane-A. J. Am. Chem. Soc. **2006**, 128(16):5533-5540.
**75.** Jose KVJ, Beckett D, Raghavachari K. Vibrational circular dichroism spectra for large molecules through molecules-in-molecules fragment-based approach. J. Chem. Theory. Comput. **2015**, 11(9):4238-4247.
**76.** Reiter, K, Kuhn, M, Weigend F. Vibrational Circular Dichroism Spectra for large molecules and molecules with heavy elements. J. Chem. Phys. **2017**, 146:054102.
**77.** Brotin T, Cavagnat D, Buffeteau T. Conformational changes in cryptophane having $C_1$-symmetry studied by vibrational circular dichroism. J. Phys. Chem. A **2008**, 112(36):8464–8470.
**78.** Daugey N, Brotin T, Vanthuyne N, Cavagnat D, Buffeteau T. Raman optical activity of enantiopure cryptophanes. J. Phys. Chem. B **2014**, 118(19):5211-5217.
**79.** Jose KVJ, Raghavachari K. Raman optical activity spectra for large molecules through molecules-in-molecules fragment based approach. J. Chem. Theory. Comput. **2016**, 12(2):585-594.
**80.** Wenzel TJ, Wilcox JD. Chiral reagents for the determination of enantiomeric excess and absolute configuration using NMR spectroscopy. Chirality: The Pharmacological, Biological, and Chemical Consequences of Molecular Asymmetry **2003**, 15(3):256-270.
**81.** Harada N. Determination of absolute configurations by X-ray crystallography and $^1$H NMR anisotropy. Chirality: The Pharmacological, Biological, and Chemical Consequences of Molecular Asymmetry **2008**, 20(5):691-723.
**82.** Seco JM, Quinoá E, Riguera R. The assignment of absolute configuration by NMR. Chem. Rev. **2004**, 104(1):17-118.
**83.** Bartik K, El Haouaj M, Luhmer M, Collet A, Reisse J. Can monoatomic xenon become chiral? ChemPhysChem, **2000**, 4:221-224.
**84.** Gomez ED, Brotin T, Duddeck H. Enantiodifferentiation of polyethers by the dirhodium method. Part 2: Cyclotriveratrylenes and cryptophanes. Tetrahedron Asym. **2007**, 18:2155-264.
**85.** Polavarapu PL. Why is it important to simultaneously use more than one chiroptical spectroscopic method for determining the structures of chiral molecules? Chirality **2008**, 20(5):664-672.
**86.** Polavarapu PL. Molecular structure determination using chiroptical spectroscopy: Where we may go wrong? Chirality **2012**, 24(11):909-920.
**87.** Nicu VP, Mandi A, Kurtan T, Polavarapu PL. On the complementarity of ECD and VCD techniques. Chirality **2014**, 26(9):525-531.
**88.** At that time it was not established that $CHCl_3$ could enter or not the cavity of these cryptophane hosts. Nowadays, it is clearly established that $CHCl_3$ easily enters the cavity of the cryptophane-C host and acts as a competitor with guest molecules.
**89.** Costante-Crassous; J., Marrone; T.J., Briggs; J.M., McCammon, J.A.; Collet, A. Absolute configuration of Bromochlorofluoromethane from Molecular Dynamics Simulation of its Enantioselective Complexation by Cryptophane-C. J. Am. Chem. Soc. **1997**, 119(16): 3818-3823.
**90.** Costante J, Hecht L, Polavarapu PL, Collet A, Barron LD. Absolute configuration of bromochlorofluoromethane from experimental and ab initio theoretical vibrational raman optical activity. Angew. Chem.**1997**, 36(8):885-887.
**91.** Bouchet A, Brotin T, Linares M, Ågren H, Cavagnat D, Buffeteau T. Enantioselective complexation of chiral propylene oxide by an enantiopure water-soluble cryptophane. J. Org. Chem. **2011** 76(10):4178-4181.
**92.** Bouchet A, Brotin T, Linares M, Cavagnat D, Buffeteau T. Influence of the chemical structure of water-soluble cryptophanes on their overall chiroptical and binding properties. J. Org. Chem. **2011**, 76:7816-7825.
**93.** De Rycke N, Jean M, Vanthuyne N, Buffeteau T, Brotin T. Enantioselective complexation of chiral oxirane derivatives by an enantiopure cryptophane in water. Eur. J. Org. Chem. **2018**, 2018(13):1601-1607.
**94.** Haberhauer G, Woitschetzki S, Bandmann H. Strongly underestimated dispersion energy in cryptophanes and their complexes. Nature Commun. **2014**, 5:3542.
**95.** Brotin T, Linares M, Ågren H, Cavagnat D, Buffeteau T. Conformational effects induced by guest encapsulation in an enantiopure water-soluble cryptophane. J. Org. Chem. **2011**, 76(5):1372-1383.
**96.** Mough ST, Goeltz JC, Holman KT. Isolation and structure of an "Imploded" cryptophane. Angew. Chem. Int. Ed. **2004**, 43(42):5631-5635.
**97.** Huber G, Brotin T, Dubois L, Desvaux H, Dutasta J.P, Berthault P. Water soluble cryptophanes showing unprecedented affinity for xenon: candidates as NMR-based biosensors. J. Am. Chem. Soc. **2006**, 128(18):6239-6246.
**98.** Warnke I, Furche F. Circular dichroism: electronic. Wiley Interdiscip. Rev. Comp. Mol. Sc. **2012**, 2(1):150–166.
**99.** Mukhopadhyay P, Zuber G, Goldsmith M-R, Wipf P, Beratan DN. Solvent Effect on Optical Rotation: A Case Study of Methyloxirane in Water. ChemPhysChem **2006**, 7:2483-2486.
**100.** Mukhopadhyay P, Zuber G, Wipf P, Beratan DN. Contribution of a Solute's Chiral Solvent Imprint to Optical Rotation. Angew. Chem. Int. Ed. **2007**, 46:6450-6452.
**101.** Bartik K, Luhmer M, Dutasta JP, Collet A, Reisse J. $^{129}$Xe and $^1$H NMR study of the reversible trapping of xenon by cryptophane-A in organic solution. J. Am. Chem. Soc. **1998**, 120(4):784–791.
**102.** Garcia S, Chavez L, Lowery T.J. Han, S. I. Wemmer, D. E. Pines, A. Sensitivity enhancement by exchange mediated magnetization transfer of the xenon biosensor signal. J. Magn. Reson. **2007**, 184(1):72–77.
**103.** Hilty C, Lowery T.J, Wemmer D. E, Pines A. Spectrally Resolved Magnetic Resonance Imaging of a Xenon Biosensor. Angew. Chemie - Int. Ed. **2005**, 45(1):70–73.
**104.** Seim, K. L.; Palaniappan, K. K.; Francis, M. B.; Meldrum, T.; Wu, W.; Pines A, Wemmer D.E, Bajaj V.S, A xenon-based molecular sensor Assembled on an MS2 viral capsid scaffold. J. Am. Chem. Soc. **2010**, 132(17):5936–5937.
**105.** Ramirez R. M, Francis M. B, Palaniappan K. K, Wemmer D. E, Bajaj V. S, Pines A. Molecular imaging of cancer cells using a bacteriophage-based $^{129}$Xe NMR biosensor. Angew. Chemie Int. Ed. **2013**, 52 (18):4849–4853.
**106.** Boutin C, Stopin A, Lenda F, Brotin T, Dutasta J. P., Jamin N, Sanson A, Boulard, Y, Leteurtre F, Huber G, Bogaert-Buchmann A, Tassali N, Desvaux H, Carrière M, Berthault P. Cell uptake of a biosensor detected by hyperpolarized $^{129}$Xe NMR: The transferrin case. Bioorg. Med. Chem. **2011**, 19(13):4135–4143.
**107.** Khan N.S, Dmochowski I.J, Bai Y, Riggle B. A, Seward G. K, Cryptophane-folate biosensor for $^{129}$Xe NMR. Bioconjug. Chem. **2014**, 26(1):101–109.
**108.** Fairchild RM, Joseph AI, Holman KT, Fogarty HA, Brotin T, Dutasta JP, Boutin C, Huber G, Berthault P. A water-soluble Xe@cryptophane-111 complex exhibits very high thermodynamic stability and a peculiar $^{129}$Xe NMR chemical shift. J. Am. Chem. Soc. **2010**, 132(44):15505–15507.
**109.** Luhmer M, Godson BM, Song YQ, Laws DD, Kaiser L, Cyrier MC, Pines A. Study of xenon binding in cryptophane-A using laser-induced NMR polarization enhancement. J. Am. Chem. Soc. **1999**, 121(14):3502-3512.
**110.** Brotin T, Devic T, Lesage A, Emsley L, Collet A. Synthesis of deuterium-labeled cryptophane-A and investigation of Xe@cryptophane complexation dynamics by 1D-EXSY NMR experiments. Chem. Eur. J. **2001**, 7(7):1561–1573.
**111.** Ruiz EJ, Sears DN, Pines A, Jameson CJ. Diastereomeric Xe chemical shifts in tethered cryptophanes cages. J. Am. Chem. Soc. **2006**, 128(51):16980-16988.
**112.** Huber JG, Dubois L, Desvaux H, Dutasta JP, Brotin T, Berthault P. NMR study of optically active monosubstituted cryptophanes and their interaction with xenon. J. Phys. Chem. A **2004**, 108(44):9608-9615.
**113.** Taratula O, Bai Y, D'Antonio E, Dmochowski I.J. Enantiopure cryptophane-$^{129}$Xe nuclear magnetic resonance biosensors targeting carbonic anhydrase. Supra. Chem. **2015**, 27:65-71.
**114.** Kotera N, Tassali N, Léonce E, Boutin C, Berthault P, Brotin T, Dutasta, JP, Delacour L, Traoré, T, Buisson, DA, Taran, F, Coudert, S, Rousseau B. A Sensitive Zinc-Activated $^{129}$Xe MRI Probe. Angew. Chem. Int. Ed. **2012**, 51(17):4100-4103.

**115.** Tassali N, Kotera N, Boutin C, Léonce E, Boulard Y, Rousseau, B, Dubost, E, Taran, F, Brotin, T, Dutasta, J.-P, Berthault P. Smart Detection of Toxic Metal Ions, $Pb^{2+}$ and $Cd^{2+}$, Using a $^{129}Xe$ NMR-Based Sensor. Anal. Chem. **2014**, 86(3): 1783-1788.
**116.** Kotera N, Dubost E, Milanole G, Doris E, Gravel E, Arhel N, Brotin T, Dutasta JP, Cochrane J, Mari E, Boutin C, Léonce E, Berthault P, Rousseau B. A doubly responsive probe for the detection of cys4-tagged proteins. Chem. Commun. **2015**, 51:11482-11484.
**117.** Mari E, Bousmah Y, Boutin C, Léonce E, Milanole G, Brotin T, Berthault P, Erard M. Bimodal detection of proteins by $^{129}Xe$ NMR and fluoresence spectroscopy. ChemBioChem, **2019**, 20:1450-1457.
**118.** Zhang D, Ronson T. K, Greenfield J. K, Brotin T, Berthault P, Léonce E, Zhu J.-L, Xu L, Nitschke J. R. Enantiopure $[Cs^{+}/Xe \subset$cryptophane$] \subset Fe^{II}_{4}L_{4}$ hierarchical superstructures. J. Am. Chem. Soc. **2019**, 141(20):8339-8345.
**119.** Brotin T, Montserret R, Bouchet A, Cavagnat D, Linares M, Buffeteau T. High affinity of water-soluble cryptophanes for cesium cations. J. Org. Chem. **2012**, 77(2):1198-1201.
**120.** Brotin T, Cavagnat D, Berthault P, Montserret R, Buffeteau T. Water-soluble molecular capsule for the complexation of cesium and thallium cations. J. Phys. Chem. B **2012**, 116(35):10905-10914.
**121.** Brotin T, Goncalves S, Berthault P, Cavagnat D, Buffeteau T. Influence of the cavity size of water-soluble cryptophanes on their binding properties for cesium and thallium cations. J. Phys. Chem. B **2013**, 117(41):12593-12601.
**122.** Doll M, Berthault P, Léonce E, Boutin C, Buffeteau T, Daugey N, Vanthuyne N, jean M, Brotin T, De Rycke N. Are the Physical Properties of Xe@Cryptophane Complexes Easily Predictable? The Case of the *Syn* and *Anti* Tris-Aza-Cryptophanes. J. Org. Chem. **2021** DOI: 10.1021/acs.joc.1c00701